Galaxy evolution in Hickson compact groups: The role of ram pressure stripping and strangulation

Jesper Rasmussen,[1]*† Trevor J. Ponman,[2] Lourdes Verdes-Montenegro,[3] Min S. Yun[4] and Sanchayeeta Borthakur[4]

[1]*Observatories of the Carnegie Institution, 813 Santa Barbara Street, Pasadena, CA 91101, USA*
[2]*School of Physics and Astronomy, University of Birmingham, Edgbaston, Birmingham B15 2TT*
[3]*Instituto de Astrofísica de Andalucía, CSIC, Apdo. Correos 3004, E-18080 Granada, Spain*
[4]*Astronomy Department, University of Massachusetts, Amherst, MA 01003, USA*

ABSTRACT

Galaxies in compact groups tend to be deficient in neutral hydrogen compared to isolated galaxies of similar optical properties. In order to investigate the role played by a hot intragroup medium (IGM) for the removal and destruction of HI in these systems, we have performed a *Chandra* and *XMM-Newton* study of eight of the most HI deficient Hickson compact groups. Diffuse X-ray emission associated with an IGM is detected in four of the groups, suggesting that galaxy–IGM interactions are not the dominant mechanism driving cold gas out of the group members. No clear evidence is seen for any of the members being currently stripped of any hot gas, nor for galaxies to show enhanced nuclear X-ray activity in the X-ray bright or most HI deficient groups. Combining the inferred IGM distributions with analytical models of representative disc galaxies orbiting within each group, we estimate the HI mass loss due to ram pressure and viscous stripping. While these processes are generally insufficient to explain observed HI deficiencies, they could still be important for HI removal in the X-ray bright groups, potentially removing more than half of the ISM in the X-ray bright HCG 97. Ram pressure may also have facilitated strangulation through the removal of galactic coronal gas. In X-ray undetected groups, tidal interactions could be playing a prominent role, but it remains an open question whether they can fully account for the observed HI deficiencies.

Key words: galaxies: evolution — galaxies: interactions — galaxies: ISM — X-rays: galaxies — X-rays: galaxies: clusters

1 INTRODUCTION

The origin of the galaxy morphology-density relation is still one of the most important unsolved problems in astrophysics. Not only are spiral galaxies less common within dense cluster environments, but those which are present tend to be deficient in HI, and this deficiency itself correlates with projected local galaxy density (e.g., Giovanelli & Haynes 1985). The mechanisms responsible for the changes in the morphology and gas content of galaxies are unclear, with gas stripping, tidal shocks, and galaxy interactions and mergers all contenders.

Traditionally, clusters of galaxies have represented the environment of choice for attempts to unravel the nature of the relevant processes. Recent results, however, strongly suggest that the origin of the environmental modification of galaxies which underpin the morphology-density relation lies, not in the cores of galaxy clusters, but in smaller groups and cluster outskirts. For exam-

ple, spectroscopic studies of the effects of the cluster environment on galaxies (e.g., Lewis et al. 2002) show that the suppression of star formation takes place in cluster outskirts rather than in the core, and is modulated by local galaxy density. Moreover, X-ray bright groups show a morphology-density relation *stronger* than that of clusters (Helsdon & Ponman 2003), a result adding to the accumulating evidence that cluster galaxies have often been 'pre-processed' in groups prior to their assembly into larger systems (see, e.g., Cortese et al. 2006). In addition, it is becoming clear that processes once thought to be exclusive to the cluster environment, such as ram pressure stripping (Rasmussen, Ponman & Mulchaey 2006) and strangulation (Kawata & Mulchaey 2008), may play a role also in much smaller systems. In order to elucidate the origin of the morphology-density relation, it is therefore necessary to study the processes acting on galaxies within groups.

The compact groups in the catalogue of Hickson (1982) offer particularly interesting opportunities in this regard. Many of these groups are spiral-rich, but their galaxy population is, on average, deficient in HI by a factor of ~ 2 compared to loose groups (Williams & Rood 1987). Furthermore, some of these groups have

* E-mail: jr@ociw.edu
† Chandra Fellow

exceptionally compact galaxy configurations, and so may represent pre-virialisation systems close to maximum collapse, in which galaxies are suffering strong environmental modification but have yet to be converted into early-types. While recent work has identified tidal interactions and mergers as playing an important role in the morphological transformation of spirals in some compact groups (Coziol & Plauchu-Frayn 2007), it is still unclear what is causing the observed H I deficiencies and to what extent this is related to the processes modifying the stellar component of the group members.

Verdes-Montenegro et al. (2001) presented a detailed study of the H I content of a sample of 72 Hickson compact groups (HCGs), with integrated H I masses from single dish measurements, and detailed Very Large Array (VLA) mapping of a subsample. Defining H I deficiency Δ_{HI} as

$$\Delta_{\mathrm{HI}} \equiv \log M_{\mathrm{HI,pred}} - \log M_{\mathrm{HI,obs}}, \qquad (1)$$

where $M_{\mathrm{HI,obs}}$ is the observed H I mass of the group galaxies and $M_{\mathrm{HI,pred}}$ is that predicted for isolated galaxies of similar morphology and optical luminosity (Haynes & Giovanelli 1984), this work confirmed the deficiency in HCGs, and allowed a search for correlations between deficiency and other group properties. One of the strongest relationships found was that with detectable intergalactic X-ray emission; almost half of the groups with significant H I deficiency showed diffuse intragroup X-ray emission in the *ROSAT* survey of Ponman et al. (1996, hereafter P96). More recently, similar results have been reported also for groups outside Hickson's catalogue (Sengupta & Balasubramanyam 2006).

The increased prevalence of X-ray detected systems among H I deficient (compact) groups may suggest a picture whereby H I is stripped from spiral galaxies within virialising groups, and then destroyed due to heating by a surrounding hot intragroup medium (IGM). However, for most of the compact groups in the Verdes-Montenegro et al. (2001) sample, *ROSAT* data were either not available or of insufficient quality to permit any detailed study of the relationship between the hot and cold gas. With only very shallow *ROSAT* All-Sky Survey data at their disposal for a number of these systems, Verdes-Montenegro et al. (2001) could not establish the amount and properties of any hot IGM in these groups.

In order to explore the processes destroying H I in these systems, we have therefore embarked on a programme to obtain high quality X-ray and radio data for the most H I deficient compact groups, adding in existing archival X-ray data wherever relevant. Since ram pressure stripping can only operate where a significant IGM is present, while tidal stripping of gas requires only that galaxies be interacting, a key discriminator for the mechanism of H I removal from galaxies is whether or not there is a correlation between H I deficiency and the properties of a hot IGM, and in particular whether a hot IGM is present in the highly H I deficient systems. Clarifying these issues represents the goal of the present study, in an attempt to shed light on the role played by galaxy–IGM interactions in destroying H I and establishing the morphology-density relation in these compact groups. The focus of this paper thus rests mainly on the X-ray properties of any hot intergalactic gas within the groups, while a forthcoming companion paper (Verdes-Montenegro et al., in prep.) will discuss in more detail the H I and radio continuum emission in the groups, the detailed relationship between X-ray and H I morphology, and the multi-wavelength properties of the individual group galaxies.

In Sections 2 and 3 we outline the sample selection and X-ray data analysis, respectively. Section 4 presents the results for the X-ray properties of the hot gas and galaxies within each group, and compares the derived IGM properties to the observed H I deficiencies. In Section 5 we construct an analytical model of a representative late-type galaxy orbiting within the derived gravitational potential of each X-ray bright group, allowing us to evaluate the importance of ram pressure and viscous stripping for H I removal. The results are discussed in Section 6 and summarized along with the main conclusions in Section 7.

A Hubble constant of 73 km s^{-1} Mpc^{-1} is assumed throughout. Unless otherwise stated, all errors are quoted at the 68 per cent confidence level.

2   GROUP SAMPLE AND OBSERVATIONS

Our broad aim is to establish the relationship between the hot and cold gas in H I deficient groups, and explore the processes of gas removal operating within them. Our sample is therefore based on that studied by Verdes-Montenegro et al. (2001), from which we selected all HCGs which are highly deficient in H I ($\Delta_{\mathrm{HI}} > 0.5$) based on Very Large Array (VLA) H I data, contain four or more group galaxies, and lie at a distance $D < 100$ Mpc. This yielded an initial sample of 11 groups, which will be discussed in its entirety in Verdes-Montenegro et al. (in prep.). VLA H I mapping has been completed for all 11 systems, along with follow-up Green Bank Telescope (GBT) observations for the groups discussed in this paper. Compared to the VLA, the single-dish GBT is more sensitive to extended, smoothly distributed emission that may otherwise be filtered out by the VLA interferometer. Including the GBT data thus provides a more complete census of the H I content in the groups. For HCG 48, included in the initial sample, the additional gas detected by GBT indicates that this group is not H I deficient after all. Consequently, this group was omitted from the sample for the purpose of the present study.

Of the remaining systems, the eight included in this paper are those for which *Chandra* or *XMM-Newton* X-ray data are currently available. Four of these eight groups are exceptionally compact, with major galaxies (as catalogued by Hickson 1982) contained within a circle of radius ~ 2 arcmin, and thus requiring *Chandra* data to resolve their X-ray structure in the crucial region. We note that these groups are not generally mature, X-ray bright systems dominated by early-type galaxies. Such groups may contain little H I, but the H I content of their galaxies as predicted from the Haynes & Giovanelli (1984) results mentioned above is also small (zero for ellipticals and modest for lenticulars). Such groups are therefore not usually H I *deficient* according to our definition in equation (1). Our chosen systems have H I content far below that expected for their galaxy contents, and are therefore those in which the processes which destroy H I should be in active, or very recent, operation.

The observation log for the X-ray data considered in this paper is presented in Table 1, detailing the pointing coordinates for each observation (for archival observations not necessarily identical to the optical group centre), group distance D, the observing instrument, date, and mode, along with cleaned exposure times t_{exp} for each camera, and the Galactic absorbing column density N_{H} from Dickey & Lockman (1990) as adopted in the X-ray spectral analysis.

Table 1. Log of available X-ray observations. Group luminosity distances D for the adopted value of H_0 were taken from the NASA/IPAC Extragalactic Database (NED). Column 7 specifies the frame mode (full frame/extended full frame) and optical blocking filter for *XMM*, and ACIS CCD aimpoint and telemetry mode (Faint/Very Faint) for *Chandra*.

Group	RA (J2000)	Dec (J2000)	D (Mpc)	*Chandra*/ *XMM*	Obs. date (yyyy-mm-dd)	Obs. mode	$t_{\exp}$ (ks)	N_{H} (10^{20} cm^{-2})
HCG 7	00 39 13.5	+00 51 49.3	54	*XMM* pn	2004-12-26	FF Thin	25.9	2.24
…	…	…	…	*XMM* m1	…	FF Thin	35.1	…
…	…	…	…	*XMM* m2	…	FF Thin	35.9	…
HCG 15	02 07 39.0	+02 08 18.0	92	*XMM* pn	2002-01-10	EFF Thin	23.3	3.20
…	…	…	…	*XMM* m1	…	FF Thin	31.0	…
…	…	…	…	*XMM* m2	…	FF Thin	31.1	…
HCG 30	04 36 28.3	−02 50 02.9	63	*Chandra*	2006-02-07	ACIS-S VF	29.0	5.08
HCG 37	09 13 35.3	+30 01 25.5	97	*Chandra*	2005-01-13	ACIS-S VF	17.5	2.30
HCG 40	09 38 56.7	−04 50 55.9	98	*Chandra*	2005-01-29	ACIS-S VF	31.8	3.64
…	…	…	…	…	2005-01-29	ACIS-S VF	14.6	…
HCG 44	10 18 02.5	+21 48 50.7	23	*Chandra*	2002-03-14	ACIS-S F	19.4	2.16
…	10 17 38.0	+21 41 17.0	…	*XMM* pn	2001-05-07	EFF Thick	8.1	…
…	…	…	…	*XMM* m1	…	FF Thin	13.4	…
…	…	…	…	*XMM* m2	…	FF Thin	13.1	…
HCG 97	23 47 25.4	−02 19 45.5	86	*Chandra*	2005-01-14	ACIS-S VF	36.2	3.65
HCG 100	00 01 25.9	+13 06 30.4	69	*Chandra*	2006-06-12	ACIS-I VF	26.1	4.40
…	…	…	…	…	2007-01-24	ACIS-I VF	16.1	…

3 DATA REDUCTION AND ANALYSIS

3.1 *XMM-Newton* data

The *XMM* data were analysed using XMMSAS v6.5.0, and calibrated event lists were generated with the 'emchain' and 'epchain' tasks. Event files were filtered using standard quality flags, while retaining only patterns $\leqslant 4$ for pn and $\leqslant 12$ for MOS. Screening for background flares was first performed in the 10–15 keV band for MOS and 12–14 keV for pn. Following an initial removal of obvious large flares, a 3σ clipping of the resulting lightcurve was applied. Point sources were then identified by combining the results of a sliding-cell search ('eboxdetect') and a maximum likelihood point spread function fitting ('emldetect'), both performed in five separate energy bands spanning the total range 0.3–12 keV. In order to filter out any remaining soft protons in the data, a second lightcurve (3σ) cleaning was then done in the 0.4–10 keV band, within a 9–12 arcmin annulus which excluded the detected point sources. Closed-filter data from the calibration database and blank-sky background data (Read & Ponman 2003) for the appropriate observing mode were filtered similarly to source data, and screened so as to contain only periods with count rates within 1σ from the mean of the source data. All point sources were excised out to at least 25 arcsec in spectral analysis.

To aid the search for diffuse X-ray emission within the groups, smoothed exposure-corrected images were produced, with background maps generated from blank-sky data. We allowed for a differing contribution from the non-vignetted particle background component in source- and blank-sky data by adopting the following approach. First an EPIC mosaic image was smoothed adaptively (3σ–5σ significance range), and the particle background was subtracted. The latter was estimated from closed-filter data which were scaled to match source data count rates in the image energy band in regions outside the field of view, and then smoothed at the same spatial scales as the source data. The resulting photon image includes the X-ray background at the source position. To remove this component, a particle-subtracted blank-sky image was produced in a similar way, and scaled to match 0.3–2 keV source count rates in a point-source–excised 10–12 arcmin annulus assumed to be free of IGM emission (this assumption is clearly justified in all cases, as will be shown). This image was then subtracted from the corresponding source image, and the result was finally exposure-corrected.

3.2 *Chandra* data

For all *Chandra* data sets, calibrated event lists were regenerated using CIAO v3.3. For Very Faint mode observations, the standard additional background screening was carried out. Bad pixels were screened out using the bad pixel map provided by the pipeline, and remaining events were grade filtered, excluding *ASCA* grades 1, 5, and 7. Periods of high background were filtered using 3σ clipping of full–chip lightcurves, binned in time bins of length 259.8-s and extracted in off-source regions in the 2.5–7 keV band for back-illuminated chips and 0.3–12 keV for front-illuminated chips. Blank-sky background data from the calibration database were screened and filtered as for source data, and reprojected to match the aspect solution of the latter. Point source searches were carried out with the CIAO task 'wavdetect' using a range of scales and detection thresholds, and results were combined. Source extents were quantified using the 4σ detection ellipses from 'wavdetect', and these regions were masked out in all spectral analysis.

In order to produce smoothed images as for the *XMM* data, background maps were generated using blank-sky data, and scaled to match source count rates for each CCD. This scaling employed either the full-chip 10–12 keV count rates, with point sources excluded, or, where possible, count rates in the image energy band within source-free regions on the relevant CCD. The background maps were then smoothed to the same spatial scales as the source data and subtracted from the latter. The resulting images were finally exposure corrected using similarly smoothed, spectrally weighted exposure maps, with weights derived from spectral fits to the integrated diffuse emission (where possible, otherwise the exposure maps were weighted by a $T = 1$ keV, $Z = 0.3$ Z$_\odot$ thermal plasma model).

3.3 Spatial and spectral analysis

While the smoothed X-ray images described above are useful in terms of establishing the presence and rough morphology of any intragroup medium, we emphasize that they were used for illustrative purposes only and not for quantitative analyses. Where IGM emission was not immediately obvious from these images, we performed an additional source detection procedure based on Voronoi tessellation and percolation ('vtpdetect' in CIAO), which can be useful for detecting extended, low–surface brightness emission missed by our standard detection algorithms. To reduce the fraction of spurious detections, a minimum of 50 net counts were required for a source to be considered real.

As a second step in the search for group-scale diffuse emission, we also extracted exposure-corrected 0.3–2 keV surface brightness profiles from the unsmoothed data, with all detected point-like and extended galactic sources masked out. The profiles were extracted from the optical group centre defined by the principal members in the Hickson (1982) catalogue. For *XMM* data, we used an EPIC mosaic image for this purpose, with the particle background removed using the method described above. The estimated particle level shows a typical standard error of the mean of ≈ 5 per cent, which should be representative of the uncertainty associated with particle subtraction if the ratio of particle events inside and outside the field of view is similar to that in the closed-filter data. We used the blank-sky background data to confirm this assumption (since these have very little source contamination), but have conservatively added a 10 per cent error in quadrature to our *XMM* surface brightness errors, to allow for any residual systematic uncertainties associated with the particle subtraction.

For the spectral analysis of any extended emission, X-ray spectra were accumulated in energy bins of at least 20 net counts, and fitted in XSPEC v11.3 assuming an APEC thermal plasma model with the solar abundance table of Grevesse & Sauval (1998). *XMM* background spectra were extracted by means of the common 'double-subtraction' technique (Arnaud et al. 2002), using blank-sky background data for the on-chip background, and a large-radius (10–12 arcmin) annulus for determining the local soft X-ray background. Owing to the smaller field of view, a similar approach was not generally possible or desirable for the *Chandra* observations where source emission may completely fill the CCD under investigation. The extraction of *Chandra* background data products are therefore described individually for each group in the next Section.

Surface brightness profiles of the X-ray detected groups were extracted from the peak of the diffuse X-ray emission when clearly identifiable (in HCG 37 and 97) and from the centroid otherwise (HCG 15 and 40). The profiles were fitted with standard β–models for conversion into IGM density profiles under the assumption of isothermality. Since X-ray emissivity is very nearly independent of temperature for a $T \sim 0.5$–1 keV plasma of the relevant metallicities (see Sutherland & Dopita 1993), this approach is entirely adequate for our purposes, where the uncertainties of our analysis will ultimately be dominated by those related to the modelling of the *impact* of the hot gas on the galaxies. The density profiles were normalized using the spectral normalization A from XSPEC,

$$A = \frac{10^{-14}}{4\pi D^2(1+z)^2} \int_V n_e n_H \, dV \ \text{cm}^{-5}, \tag{2}$$

where D is the assumed group distance, and n_e and n_H are the number densities of electrons and hydrogen atoms, respectively. The integral represents the fitted emission integral I_e over the covered volume V, assumed to be spherically symmetric. Total gas masses within the region of interest were derived by simple volume integration of $n_e(r)\mu_e m_p$, where m_p is the proton mass and we have assumed $n_e/n_H = 1.165$ and $\mu_e = 1.15$, appropriate for a fully ionized $Z = 0.3$ $Z_\odot$ plasma at the relevant temperatures (Sutherland & Dopita 1993).

Since we have no knowledge of the density distribution of any hot gas in the X-ray undetected groups, we have only derived constraints on their *mean* electron density $\langle n_e \rangle$ within the region considered, effectively assuming a uniform IGM distribution. The advantage of this approach is that it provides very conservative upper limits to the IGM masses (and mean ram pressures) within the relevant region. The derived limits to $\langle n_e \rangle$ and $M_{\rm IGM}$ for these groups were obtained from the IGM count rate limits and thus depend on the depth of the X-ray data. These count rate limits were established on the basis of the exposure-corrected (and, in the case of *XMM*, particle-subtracted) images, by comparing the emission level within a region centred on the optical group centre with that in a surrounding annulus. The physical extent of the region of interest was thus constrained by the need to evaluate the background locally from our data, and varies from 50–150 kpc among the groups, as detailed in the discussion of individual groups below. The derived constraints on IGM count rates were translated into constraints on I_e, assuming the cooling function $\Lambda(T, Z)$ of Sutherland & Dopita (1993) and an IGM temperature taken from the σ_V–T_X relation of Osmond & Ponman (2004),

$$\log \sigma_V = (1.15 \pm 0.26) \log T_X + 2.60 \pm 0.03, \tag{3}$$

with galaxy velocity dispersions σ_V in km s^{-1} and T_X in keV. Errors on T were derived from the dispersion of this relation, with σ_V taken from P96 for HCG 7, 30, 37, 44, and 100, from Mahdavi et al. (2005) for HCG 97, and from Osmond & Ponman (2004) for the remainder. The resulting temperature range was then used to estimate 3σ upper limits on $\langle n_e \rangle \sim (I_e/V)^{1/2}$ inside the assumed spherical volume V for any subsolar metallicity Z. The assumption of a uniform IGM in these groups implies that we can identify the upper limit to the central IGM density n_0 with $\langle n_e \rangle$ and constrain the IGM masses by simply multiplying $\langle n_e \rangle$ and V.

In order to briefly investigate the level of nuclear X-ray activity among individual group members, 0.3–2 keV count rates of all galactic central point sources were also extracted, adopting extraction regions of 2 and 15 arcsec radius for *Chandra* and *XMM* data, respectively. In the majority of cases, photon statistics were insufficient to allow robust spectral fitting for individual sources. For consistency, all point source count rates were therefore converted to luminosities assuming a power-law spectrum of photon index $\Gamma = 1.7$, absorbed by the Galactic value of N_H. The associated uncertainties were derived from the Poisson errors on the photon count rates.

4 RESULTS

In this section we discuss the results obtained for the IGM in each group and for the X-ray emission associated with individual group galaxies. Figure 1 shows contours of the smoothed, background-subtracted X-ray emission of each group overlaid on Digitized Sky Survey (DSS) images. Diffuse X-ray emission associated with an intragroup medium is detected in four of the eight groups, as described for each group individually below. For the remaining four, we do not detect any extended group emission, neither inside a given physical radius from the optical group centre when compared to the emission level in surrounding regions, nor on the basis of the
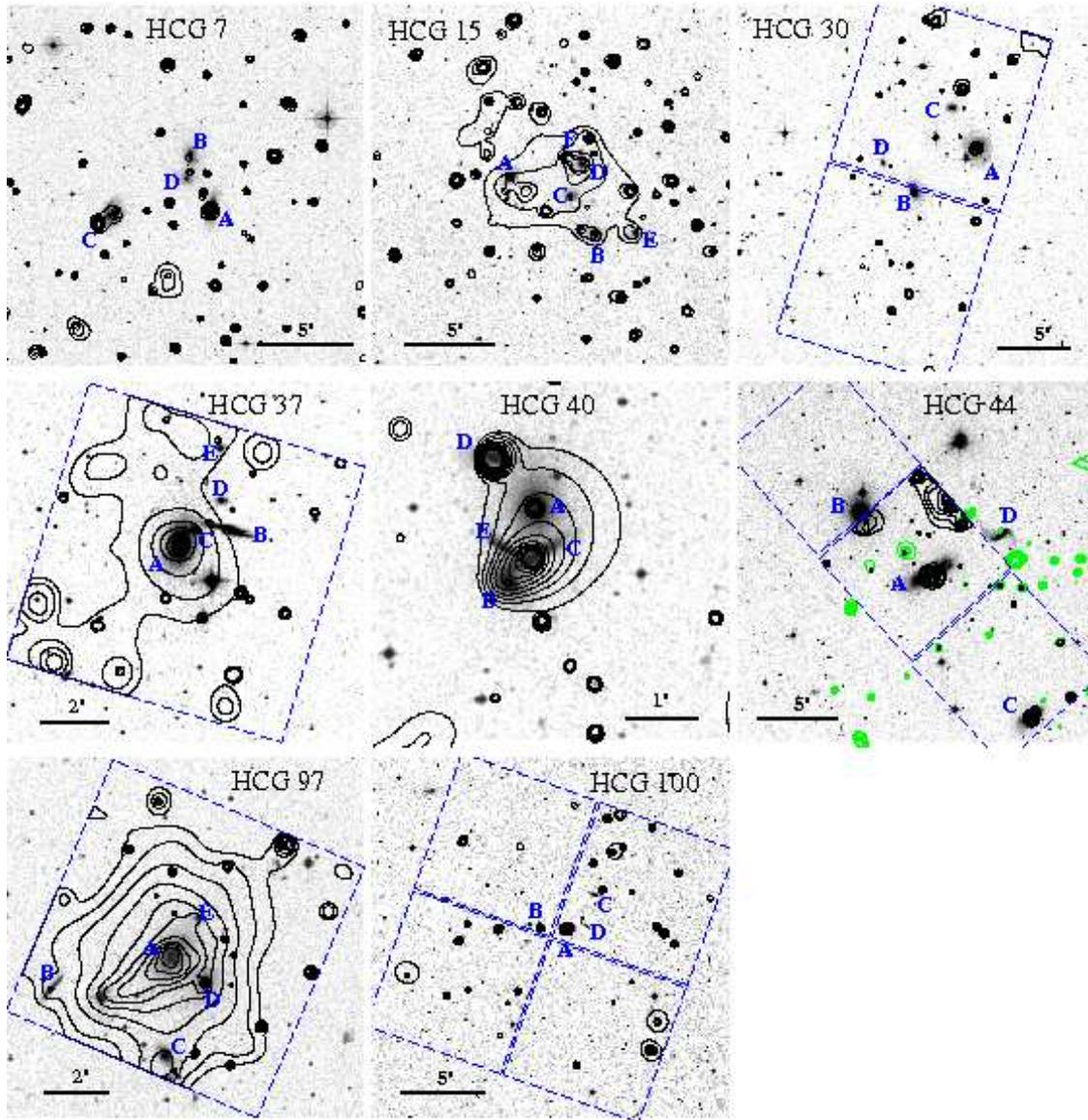
Figure 1. Contours of adaptively smoothed 0.3–2 keV emission overlayed on DSS images for all groups, with the principal group members labelled following the notation of Hickson (1982). Where relevant, dashed squares outline the coverage of the *Chandra*/ACIS CCD's. For HCG 44, dark (black) contours outline the *Chandra* emission, and lighter (green) those of an overlapping *XMM* pointing.

Voronoi source detection procedure. To corroborate these results, Figures 2 and 3 show the derived surface brightness profiles for the groups with and without detectable intragroup emission, respectively.

Table 2 summarizes the observed H I and X-ray properties of the groups, along with the adopted velocity dispersions from optical spectroscopy. H I deficiencies in the Table are from our GBT measurements (Borthakur et al., in prep.), except for HCG 44, for which we have adopted the older VLA value (Verdes-Montenegro et al. 2001) due to the GBT beam size only covering the central region of this relatively nearby system. The listed H I deficiencies are based on the integrated H I mass within the circular region covered by the radio data (r_{HI} in the Table). In many groups, a significant fraction of the detected H I is located outside the optical extent of individual galaxies (i.e. is intergalactic) and cannot be clearly assigned to any individual group member. The derived values of Δ_{HI} should

therefore generally be viewed as an average for the galaxies within the GBT or VLA field. As the fractional 1-σ uncertainty on the measured H I masses from our GBT data is less than 1 per cent for all groups, uncertainties on the listed deficiencies are dominated by those related to the predicted logarithmic H I mass, which we have taken to be 0.2, adopting the standard estimate of error provided by Haynes & Giovanelli (1984).

For reference, 0.3–2 keV X-ray luminosities are also listed in Table 2, corrected for Galactic absorption, and derived within the region employed for the spectral analysis unless otherwise specified in the subsection for the relevant group. The listed central hot IGM densities (or upper limits to the mean densities for the X-ray undetected groups) were computed as outlined in Section 3.3. IGM masses in the Table were derived within the same region as the H I deficiencies (i.e. within r_{HI} given in the Table), to enable a direct comparison between the two. Note, as indicated above, that

Table 2. Summary of derived group properties. Except where indicated, H I deficiencies Δ_{HI} are from GBT data (Borthakur et al., in prep.), obtained inside a radius r_{HI}. Column 7 lists the derived constraints on central hot IGM density, with upper limits for the X-ray undetected groups given at 3σ significance, and Column 8 the corresponding hot IGM mass within r_{HI}.

| Group	Δ_{HI}	r_{HI} (kpc)	σ_V (km s^{-1})	T_X (keV)	L_X (10^{40} erg s^{-1})	n_0 (10^{-3} cm^{-3})	M_{IGM} (10^{10} M$_\odot$)
HCG 7	0.60	68	95[a]	0.3 ± 0.1*	< 0.5	< 0.06	< 0.26
HCG 15	0.46	113	404[b]	$0.83^{+0.09}_{-0.06}$	32 ± 2	4.4 ± 0.5	7.4 ± 0.8
HCG 30	1.37	79	72[a]	0.2 ± 0.1*	< 1.3	< 1.2	< 8.3
HCG 37	0.33	119	446[a]	$0.86^{+0.13}_{-0.09}$	16 ± 2	38 ± 6	6.5 ± 1.0
HCG 40	0.60	121	157[b]	$0.59^{+0.11}_{-0.12}$	3.1 ± 0.5	1.1 ± 0.2	2.4 ± 0.4
HCG 44	0.69[†]	101	145[a]	0.4 ± 0.1*	< 3.6	< 0.1	< 1.4
HCG 97	0.35	106	383[c]	$0.97^{+0.14}_{-0.12}$	120^{+20}_{-24}	48 ± 2	13.8 ± 0.6
HCG 100	0.27	86	100[a]	0.3 ± 0.1*	< 3.4	< 0.33	< 2.9

[†] From VLA data (Verdes-Montenegro et al. 2001).
* Obtained from the assumed σ_V–T_X relation, equation (3).
[a] Ponman et al. (1996).
[b] Osmond & Ponman (2004).
[c] Mahdavi et al. (2005).
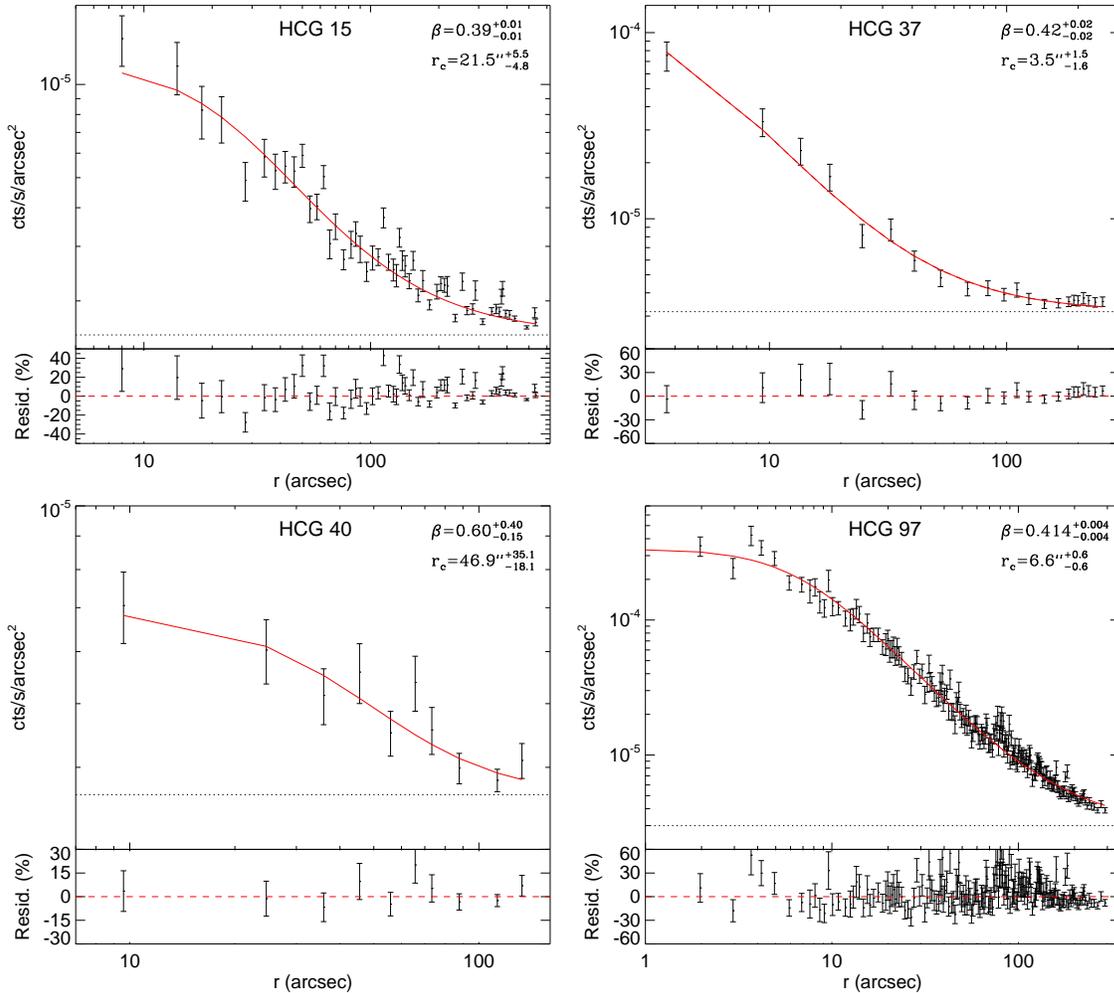
Figure 2. 0.3–2 keV exposure-corrected surface brightness profiles of groups with detectable diffuse emission, along with best-fitting β–models (solid lines). Horizontal dotted lines mark the estimated background level in each case. For each plot, the bottom panel shows fit residuals relative to the best-fitting model.
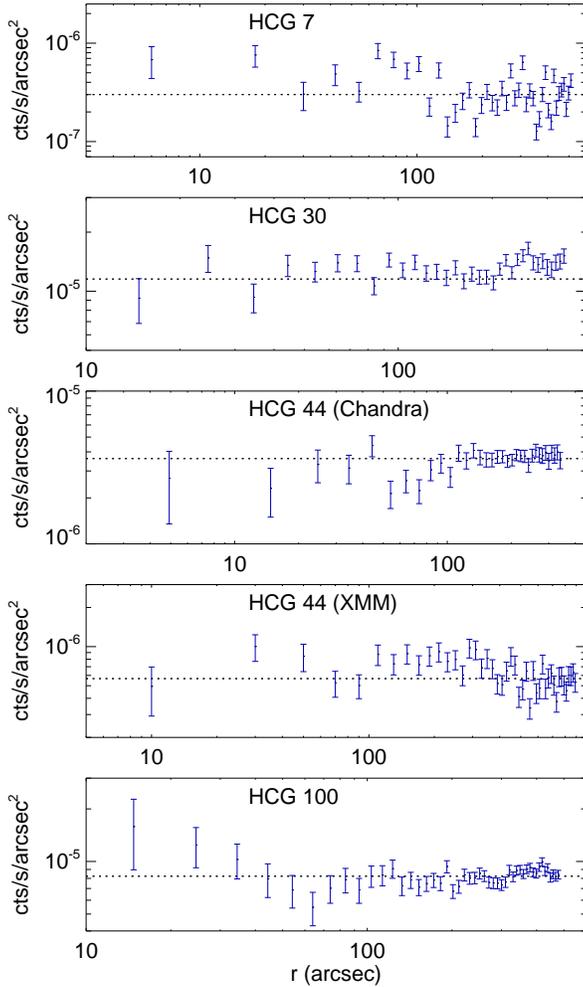
Figure 3. As Fig. 2, but for the groups without detectable diffuse emission.

the upper limits to $M_{\rm IGM}$ for the X-ray undetected groups conservatively assume a uniform IGM distribution. If instead assuming a standard β–model for the hot gas in these groups, with central density equal to the inferred mean value $\langle n_e \rangle$ and with typical group values of, e.g., $\beta = 0.5$ and $r_c = 20$ kpc, the derived IGM mass limits would be reduced by factors of 4–7.

4.1 X-ray properties of the intragroup medium

4.1.1 HCG 7

This group remained X-ray undetected in shallow *ROSAT* All-Sky Survey (RASS) data. Despite the *XMM* data of this target representing the deepest X-ray observation within our sample, no diffuse X-ray emission is detected in the group when comparing the emission level of the exposure-corrected and particle-subtracted 0.3–2 keV mosaic image inside $r = 9$ arcmin ($r \approx 140$ kpc) with that measured in a surrounding annulus. This is corroborated by the derived surface brightness profile shown in Fig. 3. Although this profile does seem to hint at a weak signal inside $r \approx 2$ arcmin, the combined signal inside this region is significant at less than 1.8σ, is not picked up by 'vtpdetect', and is not discernible in the smoothed image presented in Fig. 1. Thus, we conservatively treat it as a non-detection.

In fact, no extended emission unassociated with individual galaxies is identified by 'vtpdetect' within the 9 arcmin radius, with the exception of the source visible in Fig. 1 roughly ~ 5 arcmin south of the optical group centre. There are no optical/infra-red counterparts to this X-ray source listed in NED within a 2 arcmin diameter, despite the proximity of the group ($D \approx 54$ Mpc). The emission is detected out to 2.2 arcmin from the X-ray centroid at 3σ above the local background, confirming that it is clearly extended. A thermal plasma model fit to the spectrum extracted from the pn data within $r = 1.5$ arcmin of the centroid provides an acceptable fit, with a reduced $\chi_\nu^2 = 0.92$ for 24 degrees of freedom (d.o.f.). This yields a best-fitting temperature $T = 2.6^{+0.7}_{-0.4}$ keV and redshift $z = 0.41^{+0.12}_{-0.02}$ for an assumed abundance of 0.3 solar. A simple power-law model with Galactic absorption yields $\Gamma = 1.84 \pm 0.10$ for the power-law index, but the fit is not preferred to a thermal model (red. $\chi_\nu^2 = 1.07$ for 25 d.o.f, i.e. a change of $\Delta\chi^2 = 4.8$). The estimated temperature can be compared to that expected for the IGM in HCG 7 on the basis of its very low galaxy velocity dispersion, $\sigma_{\rm V} = 95$ km s^{-1}, for which the $\sigma_{\rm V}$–$T_{\rm X}$ relation of Osmond & Ponman (2004) would suggest only $T = 0.3 \pm 0.1$ keV. Combined with the redshift estimate of $z \approx 0.4$, this strongly suggests that this emission is not associated with HCG 7 itself. The X-ray centroid also coincides to within 10 arcsec with an NVSS source with a 1.4 GHz flux of 19.4 mJy (corresponding to 1×10^{25} W Hz^{-1} at $z = 0.41$), so the X-ray emission is conceivably associated with a $z \approx 0.4$ background cluster harbouring a central radio-loud galaxy.

For T anywhere in the range 0.2–0.4 keV and assuming any subsolar metallicity, our failure to detect IGM emission inside $r \approx 150$ kpc translates into a 3σ upper limit to the unabsorbed 0.3–2 keV luminosity inside this region of $L_{\rm X} < 5 \times 10^{39}$ erg s^{-1}, with a corresponding limit to the mean gas density of $\langle n_e \rangle < 6 \times 10^{-5}$ cm^{-3}. We note that HCG 7 is included in the group catalogue of Yang et al. (2007), with a total group mass, as estimated from its optical properties, ranging from 2.4–5.0$\times 10^{12}$ M$_\odot$ depending on the method assumed. This places HCG 7 at the very low-mass end of the group mass function, with a mass similar to that of the Local Group. Thus, it is perhaps not surprising that we fail to detect any IGM emission in this system.

4.1.2 HCG 15

This group has a relatively high velocity dispersion of $\sigma_{\rm V} \approx 400$ km s^{-1}, and hot intragroup gas was already detected in pointed *ROSAT* observations (P96). Significant IGM emission is seen in the *XMM* data presented in Fig. 1, revealing a somewhat disturbed X-ray morphology. Despite this irregularity of the emission, an optically bright early-type galaxy is present roughly at centre of the X-ray emission, as is typical for fairly undisturbed X-ray bright groups. The facts that this galaxy is a lenticular rather than an elliptical, and that the IGM emission is not (yet) strongly peaked on this galaxy, may suggest that the group is in the late stages of dynamical relaxation.

Emission is detected in the imaging data out to $r = 8.9$ arcmin ($r \approx 230$ kpc) at 5σ above the X-ray background level evaluated from a surrounding annulus. A radial surface brightness profile is shown in Fig. 2, extracted from the centroid of emission in bins containing a signal-to-noise ratio of S/N $\geqslant 5$. As expected from the irregular X-ray morphology, a standard β–model is not a satisfactory description of this profile, with χ_ν^2 of 3.5 for 52 d.o.f. The data show significant deviations from the best-fitting model (with $\beta = 0.39 \pm 0.01$ and $r_c = 21.5^{+5.5}_{-4.8}$ arcsec) at all radii. However,

the fit residuals do not exhibit any systematic radial variation, suggesting they are caused by local fluctuations in the IGM distribution rather than large-scale inhomogeneities. Hence, despite the fact that the β–model fit is clearly statistically unacceptable, it remains useful for our purposes as a means of characterizing the global hot gas distribution. From inspection of Fig. 2, it is also not clear that a different, or more complex, model would be able to provide a better description.

The relatively broad point spread function (PSF) of *XMM*, not accounted for in the surface brightness fitting, could potentially affect the observed profile at small radii, and hence the derived core radius and central gas density. We do not expect this to be an important effect, however, because even just the innermost radial bin in Fig. 2 extends to $r = 12$ arcsec, roughly twice the full-width at half maximum of the EPIC PSF. The fact that the best-fitting core radius is another factor of two larger also suggests that PSF blurring does not have a significant impact on the derived results.

Using the double-subtraction approach for extracting a background spectrum, a fit to the global 0.3–5 keV spectrum extracted inside $r = 6$ arcmin ($r = 150$ kpc) gives a temperature $T = 0.83^{+0.09}_{-0.06}$ keV and abundance $Z = 0.03 \pm 0.01$ $Z_\odot$, thus confirming the low abundance derived from *ROSAT* data within the same region (Osmond & Ponman 2004). These values are consistent with those obtained using local background subtraction, but results are better constrained due to the superior statistics of the blank-sky background data. The derived flux and surface brightness profile imply a central hot gas density $n_0 = 4.4 \pm 0.5 \times 10^{-3}$ cm^{-3}.

4.1.3 HCG 30

Despite this group representing the most HI deficient system within our sample, the *Chandra* data do not reveal any clear evidence for diffuse IGM emission. No extended sources outside individual galaxies are detected by 'vtpdetect', thus corroborating the RASS-based result of P96. With a galaxy velocity dispersion of only 72 km s^{-1}, the Osmond & Ponman (2004) scaling relations would suggest a very low IGM temperature of $T = 0.2 \pm 0.1$ keV. In order to test for the presence of any such gas, we generated 0.2–0.4 keV images of the data on the S2 and S3 CCDs separately. These images were exposure-corrected and smoothed but not background-subtracted, in an attempt to suppress any bias related to ACIS calibration uncertainties at these low energies. The results reveal no clear spatial variations in the diffuse emission on either chip, suggesting emission at a level consistent with the local background.

As a further test, we searched the unsmoothed data for a radial gradient in the exposure-corrected 0.3–2 keV emission level across the S2 and S3 CCD's, finding no significant variation with distance from the optical group centre (see Fig. 3 for a surface brightness profile extracted on the S3 CCD). This implies that any diffuse IGM emission would have to be near-uniformly distributed on scales of ~ 300 kpc, an unlikely scenario for this low-σ system, in which the angular extent of the region encompassing the four principal group members is only ≈ 5 arcmin (~ 90 kpc).

The RASS 0.5–0.9 keV count rate in a 0.5–1 deg annulus centred on the optical group centre is 8σ above the exposure-weighted mean of the appropriate *Chandra* blank-sky data, suggesting a considerable contribution from either background or (Galactic) foreground emission at this position. The high background rate relative to blank-sky data requires us to evaluate the background from the source data, thus restricting the source region under investigation on S3 to within $r \sim 3$ arcmin (~ 50 kpc) of the optical group centre. Assuming that the background in the data can be safely evalu-

ated from source-free regions on S3 outside this central region (an assumption supported by Fig. 3), the density of any hot IGM in the group can be constrained. Inside this region, and for T in the range 0.1–0.3 keV and any subsolar metallicity, the 3σ upper limit to the mean gas density is $\langle n_e \rangle < 1.2 \times 10^{-3}$ cm^{-3}. The possibility that T is very low in this group propagates into a relatively weak constraint on $\langle n_e \rangle$.

4.1.4 HCG 37

Irregular diffuse X-ray emission was detected in this group with *ROSAT* out to $r \sim 8$ arcmin (Mulchaey et al. 2003), well beyond the region covered by a single ACIS chip in our *Chandra* data. The latter clearly indicate that the group emission is sharply peaked on the early-type galaxy HCG 37a ($=$ NGC 2783), the nucleus of which is also detected as a point-like source in the data. The association of the IGM X-ray peak with HCG 37a was not obvious from the earlier *ROSAT* data, as the much broader *ROSAT* PSF required Mulchaey et al. (2003) to exclude point-like emission out to $r = 1.5$ arcmin from the peak, thus effectively masking out HCG 37a in the data. Despite the overall irregularity of the group emission, the X-ray centroid (when masking out the HCG 37a nucleus) coincides to within 10 arcsec with the optical position of HCG 37a as listed in NED.

Since group emission covers the S3 CCD, we cannot reliably use any method relying on source-free regions on S3 to evaluate the background in the *Chandra* data. The situation is aggravated by the fact that RASS data indicate a 3σ soft background deficit at this position relative to the appropriate blank-sky data, so background subtraction by means of these is not straightforward either. To circumvent these issues, we adopted the method employed by Vikhlinin et al. (2005). First, a source minus blank-sky spectrum was extracted on the back-illuminated S1 chip, to quantify the difference in the soft background between source- and blank-sky data. The spectrum was fitted with a $T = 0.18$ keV $Z = Z_\odot$ mekal plasma in the 0.4–1 keV range, with the normalization allowed to be negative. The best-fitting model was then added to the model fit of the blank-sky subtracted source emission on S3 inside $r = 3.7$ arcmin ($r \approx 100$ kpc) after scaling to the source region area. The resulting background level was also used for the surface brightness analysis. We note that, at 90 per cent confidence, the best-fitting T and Z resulting from this approach, $T = 0.86^{+0.13}_{-0.09}$ keV and $Z = 0.10^{+0.08}_{-0.04}$ $Z_\odot$, are just consistent with the P96 values inside $r = 150$ kpc ($T = 0.67 \pm 0.11$ keV, $Z = 0.17 \pm 0.15$ $Z_\odot$), lending some credibility to this approach.

The surface brightness profile shown in Fig. 2 confirms the presence of emission across the full S3 CCD in the *Chandra* data. The profile was centred on the X-ray peak and extracted in bins containing at least 30 net counts. Despite the irregularity of the emission on large scales (Fig. 1), a β–model provides a good fit to the profile across the full radial range plotted in Fig. 2, yielding $\beta = 0.42 \pm 0.02$ and $r_c = 3.5^{+1.5}_{-1.6}$ arcsec, with $\chi^2_\nu = 0.80$ for 19 d.o.f. The spatial and spectral results imply a gas density in the group core of 0.038 ± 0.006 cm^{-3}.

4.1.5 HCG 40

The *Chandra* observation of this group was split into two separate pointings, so a merged event file was produced for the imaging analysis. Although undetected in a 3.6-ks *ROSAT* pointing (P96), Fig. 1 suggests the presence of diffuse emission in this group. The

centroid of this emission, with the optical extent of the individual group members masked out, is located ~ 0.5 arcmin to the NW of HCG 40c and so is not clearly associated with any individual galaxy. To test that the emission seen in Fig. 1 is truly extended and not simply due to the smoothing of point sources, a surface brightness profile of the unsmoothed, exposure-corrected emission was extracted from the centroid in bins of at least 30 net counts, with individual galaxies masked out. The result is shown in Fig. 2, with the background evaluated from off–source regions on the S3 CCD. Emission is detected above this background out to $r = 2.3$ arcmin ($r = 65$ kpc), suggesting group-scale extended emission, although the detection is only significant at $> 3\sigma$ for the innermost 30 kpc. A β–model provides an acceptable fit to this profile, with $\chi^2_\nu = 1.01$ for 7 d.o.f., yielding $\beta = 0.60^{+0.40}_{-0.15}$ and $r_c = 46.9^{+35.8}_{-18.1}$ arcsec (23^{+17}_{-9} kpc), in accordance with expectations for a typical X-ray bright group.

For the spectral analysis of this emission, spectra and response products were extracted separately for each of the two observations. The spectra were then jointly fitted within the central $r = 1$ arcmin, within which the signal allows useful constraints to be obtained, using a surrounding 2.5–3.5 arcmin annulus for background estimation. With only ~ 140 net counts, the IGM abundance remains unconstrained. Fixing Z at 0.3 solar yields $T = 0.59^{+0.11}_{-0.12}$, and T remains consistent with this for any subsolar Z. For these parameters, the observed flux translates into a central electron density of $1.1 \pm 0.2 \times 10^{-3}$ cm^{-3} and implies a diffuse 0.3–2 keV luminosity inside $r = 2.3$ arcmin of $3.1 \pm 0.5 \times 10^{40}$ erg s^{-1}.

The extent of the emission, coupled with the fact that it is not clearly centred on any group member, suggests that the emission is not due to, for example, hot gas associated with an elliptical but rather reflects the presence of a hot IGM. This interpretation would place HCG 40 among the relatively rare examples of spiral-dominated groups showing intergalactic hot gas; within Hickson's (1982) catalogue, only HCG 16, 57, and the well-studied HCG 92 (Stephan's Quintet) share similar features (e.g., Dos Santos & Mamon 1999; Fukazawa et al. 2002; Trinchieri et al. 2003). Based on the B-band luminosities of the group members, and on the L_X–L_B relations for ellipticals and normal star-forming spirals from O'Sullivan, Ponman & Collins (2003) and Read & Ponman (2001) respectively, one would expect a total galactic diffuse $L_X \approx 9 \times 10^{40}$ erg s^{-1} in the group, a factor of three larger than that found here for the intragroup emission. Although care has been taken in masking out emission from the group members, the low S/N and the compactness of the galaxy configuration implies that we cannot exclude a residual contribution to the diffuse emission from individual galaxies. A conservative approach would be to regard the association of the observed diffuse emission with an intragroup medium in HCG 40 as tentative rather than conclusive.

4.1.6 HCG 44

While Fig. 1 does not indicate the presence of any IGM emission in this system, this could simply be an artefact of the proximity of the group ($D \approx 23$ Mpc) in combination with the limited *Chandra* angular coverage, which furthermore renders quantitative analysis of the background level in the data non-trivial. Using local background subtraction could potentially produce unreliable results, as IGM emission might cover the entire ACIS array. The situation is further complicated by an enhanced particle level in the cleaned data compared to the blank-sky files, with the 10–12 keV count rate on the S3 CCD being 35 per cent higher than the correspond-

ing blank-sky value. In addition, soft Galactic 0.5–0.9 keV emission at a level of 2σ above the blank-sky data is also present at this position, so it is not obvious that blank-sky data would be an appropriate choice for background estimates.

Fortunately, the presence of an overlapping *XMM* pointing allows an independent test for the presence of diffuse emission in the group. The *Chandra* and *XMM* surface brightness profiles shown in Fig. 3 suggest no detectable IGM emission close to the optical group centre. Note that the extraction of these profiles excluded different position angles due to the optical group centre being close to the southern (northern) edge of the S3 (EPIC) CCDs, so the profiles extend in largely opposite directions on the sky. The *XMM* profile shows no systematic variation out to $r = 15$ arcmin ($r \approx 100$ kpc), remaining largely consistent with the background level evaluated outside this region in the source data. Consequently, the background level for the *Chandra* profile was estimated from the northern corners of the S3 CCD, the result suggesting no excess diffuse emission extending northwards either.

Furthermore, no extended sources that can be unambiguously associated with group emission were detected by 'vtpdetect'. In addition to the two group galaxies HCG 44a and b, a third extended X-ray source is seen on the S3 chip, clearly visible in Fig. 1 roughly four arcmin north of the spiral HCG 44a, and also seen in both the *XMM* data and in pointed *ROSAT* observations. The X-ray peak of this source coincides with a 2MASS source with $m_K = 14.31$, but there is no optical counterpart or redshift information available in NED. If this source were at the group distance, the resulting K-band luminosity of 2.1×10^8 L$_{\odot,K}$ would place it at the extreme faint end of the dwarf galaxy luminosity function, with the *ROSAT* flux implying a ratio $L_X/L_K \approx 0.013$, two orders of magnitude above typical values seen even for dwarf *starburst* galaxies (Rasmussen, Stevens & Ponman 2004). Spectral fit results provide further support for the idea that this source is unlikely to be associated with HCG 44. A thermal plasma model fixed at the group redshift returns an unacceptable fit ($\chi^2_\nu = 1.61$), whereas a significant fit improvement results when leaving z as a free parameter, yielding $\chi^2_\nu = 1.37$ for 6 d.o.f, with $T = 1.98^{+0.67}_{-0.39}$ and $z = 0.24^{+0.09}_{-0.07}$ for an assumed abundance of $Z = 0.3$ Z$_\odot$.

While the *Chandra* data are useful in terms of investigating evidence for hot gas being stripped from individual galaxies in this very nearby system, it is not clear that these data enable significant improvements on the hot IGM constraints over the existing 4.7-ks *ROSAT* pointing (with its much larger field of view enabling a more reliable background subtraction in this case). Even the *XMM* data can only probe emission from a quarter of the volume inside $r = 100$ kpc from the optical group centre, due to the latter being close to the edge of the *XMM* field of view. Using the adopted σ–T relation, which would suggest $T = 0.4 \pm 0.1$ keV, the *ROSAT* constraint of P96 on the X-ray luminosity inside $r = 150$ kpc ($L_X < 3.6 \times 10^{40}$ erg s^{-1} for our adopted distance) translates into $\langle n_e \rangle < 1.0 \times 10^{-4}$ cm^{-3} for any subsolar metallicity. The corresponding *XMM* constraint of $\langle n_e \rangle < 1.4 \times 10^{-4}$ cm^{-3} applies within a volume less than 10 per cent of that probed by *ROSAT*, so we have adopted the stronger *ROSAT* limit in Table 2.

4.1.7 HCG 97

This constitutes the most X-ray luminous system within the sample. A two-dimensional analysis of a 21-ks *XMM* observation of this group was performed by Mahdavi et al. (2005), along with optical spectroscopy identifying 37 members. Their *XMM* data show a plume stretching to the southeast, beyond the region covered by

Fig. 1. Mahdavi et al. (2005) speculate that this plume could represent gas stripped from one of the central galaxies, but the *XMM* data alone cannot establish this, and the *Chandra* data on the S2 CCD cannot improve on the situation beyond confirming the presence and overall morphology of this feature. One of the spectroscopically identified member galaxies is located within the plume but is not itself detected in either the *XMM* or *Chandra* data. On the S3 CCD, the emission appears fairly regular in Fig. 1, albeit with the central X-ray contours somewhat elongated towards the south-east. If masking out this elongated feature, the centroid of the IGM emission coincides to within 10 arcsec with the position of the optically brightest group galaxy, HCG 97a, as listed in NED.

As established already by *ROSAT* observations (e,g., Mulchaey et al. 2003), diffuse emission in this group extends well beyond the region covered by the S3 CCD, so blank-sky data were used to evaluate the background for the *Chandra* surface brightness analysis (the RASS 0.5–0.9 keV background count rate at this position is in good agreement with the corresponding exposure-weighted mean value of the blank-sky data). We note, however, that the *Chandra* observation was somewhat affected by background flares, reducing the useful exposure time from 57.9 to 36.3-ks. As for HCG 44, the background remains high after cleaning, with the 10–12 keV count rate on S3 again being 35 per cent above the blank-sky value. While bearing this issue in mind, results indicate that emission is detected above 5σ significance everywhere on the S3 chip. A fit to the exposure-corrected 0.3–2 keV surface brightness profile, extracted from the X-ray peak and shown in Fig. 2, yields $\beta = 0.414 \pm 0.004$ and $r_c = 6.6 \pm 0.6$ arcsec, with $\chi^2_\nu = 1.45$. However, while Figure 2 and the excellent agreement of these results with the best-fitting parameters of Mulchaey et al. (2003) (who find $\beta = 0.41 \pm 0.01$ and $r_c < 0.1$ arcmin) suggest that our background estimate is not seriously in error, we will nevertheless base our normalization of the density profile on the *ROSAT* results of Mulchaey et al. (2003), given the concern about the elevated particle background in the *Chandra* data. Combining their spectral results and X-ray luminosity (0.3–2 keV $L_X = 1.20^{+0.20}_{-0.24} \times 10^{42}$ erg s^{-1} for our adopted distance) with our surface brightness fit then implies a temperature $T = 0.97^{+0.14}_{-0.12}$ keV and central density of 0.048 ± 0.002 cm^{-3}, which are the values listed in Table 2.

4.1.8   HCG 100

This is a group in which the H I is clearly being stripped from the galaxies at present, with much of it pulled into a 100 kpc long tidal tail extending to the southwest from the optical group centre (Borthakur et al., in prep.). In addition, the VLA data reveal a striking H I trail extending to the east away from the group core, protruding from one of the galaxies in the field, Mrk 935. This galaxy is not included in the original Hickson (1982) catalogue, but is a group member on the basis of its projected distance from the optical group centre (6.7 arcmin $\sim$ 130 kpc) and small radial velocity difference of $\Delta v \sim 250$ km s^{-1} relative to the group mean, as listed in NED. The associated H I feature may therefore indicate ongoing stripping as the galaxy falls into the group. HCG 100 thus constitutes an excellent laboratory for the study of the processes whereby H I is removed from individual galaxies and heated. Unlike the case for the other *Chandra* observations presented here, this group was observed using the ACIS-I array, to allow the observed field to fully encompass all of the interesting H I features mentioned above.

The *Chandra* observation was split into two, so the imaging analysis proceeded as for HCG 40. The combined imaging data,

shown in Fig. 1, and the resulting surface brightness profile in Fig. 3, do not reveal any clear indications of diffuse emission above the background level as evaluated outside $r = 8$ arcmin from the corners of the ACIS-I array. Although Fig. 3 indicates a mild net excess in the two innermost bins, the signal within this region is significant at less than 1.5σ. We also note that no extended sources are detected outside individual galaxies with 'vtpdetect', and that the group also remained undetected in RASS data (P96). With the σ–T relation suggesting $T = 0.3 \pm 0.1$ keV, the absence of an IGM detection inside $r \approx 100$ kpc ($r \approx 5$ arcmin) from the optical group centre implies a 3σ upper limit on the mean IGM density of $\langle n_e \rangle < 3.3 \times 10^{-4}$ cm^{-3}.
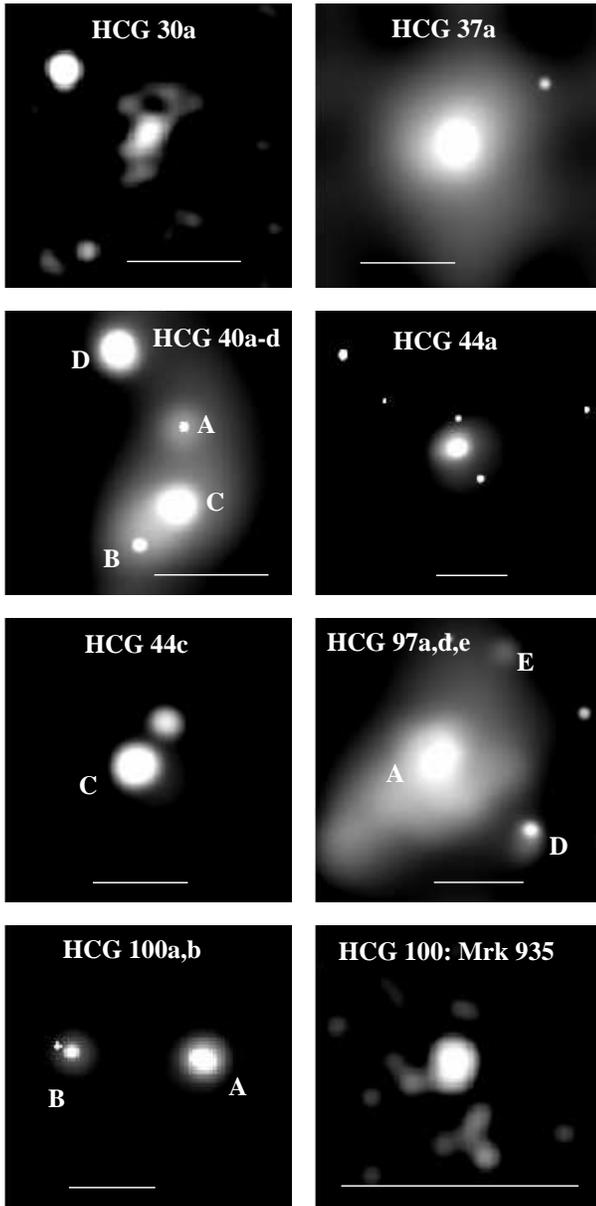
4.2   Individual galaxies

The results presented so far demonstrate the presence of a detectable hot IGM within half of our sample only. However, even in the absence of such gas, there could still be an intragroup medium present with temperature or density below our detection limits (including any H I already stripped from individual galaxies, as evidenced by the GBT detection of intergalactic H I in many of our groups).

To explore the possibility that group galaxies could be interacting with such a medium, and to search for signs of galaxies being stripped of any *hot* gas, we present in Fig. 4 a collage of all group members which were clearly identified as X-ray extended sources by our source detection algorithms. These images were adaptively smoothed following the procedure outlined in Section 3. Exceptions are HCG 30a and Mrk 935, for which a simple Gaussian smoothing (with $\sigma = 10$ arcsec) was employed due to the very low S/N. For the groups observed by *XMM* (HCG 7 and 15), the combination of group distance and the broader EPIC PSF does not enable a clear distinction between point-like and diffuse emission, so none of the relevant galaxies has been included in this figure. HCG 44b, lying on a chip gap in the *Chandra* data and not covered by the overlapping *XMM* pointing, has also been excluded.

The figure does not reveal any clear evidence for galaxies currently being stripped of any hot gas. In particular, there are no indications of X-ray tails or bow-shock features indicating interactions with a surrounding medium. Such tails have been observed extending from galaxies in clusters (e.g., Wang, Owen & Ledlow 2004; Sun & Vikhlinin 2005) but seem to be very rare in groups, with perhaps NGC 6872 and NGC 2276 the most prominent examples (Machacek et al. 2005; Rasmussen et al. 2006). There is an indication of an asymmetric structure in HCG 97d even in the unsmoothed data, with a hint of a tail pointing south, but the signal is too weak to exclude contamination by a faint point source. Mrk 935, with the remarkable H I tail extending to the east, also presents evidence of some X-ray asymmetry in this direction, but the S/N is again too low to enable firm conclusions.

In addition to diffuse galactic emission, X-ray point sources in individual galaxies are detected in all groups, with some of these sources clearly associated with the galaxy nuclei. The relevance of this is linked to the possibility that galaxies suffering strong (tidal) interactions could be showing enhanced nuclear activity, for example associated with a nuclear starburst or strong AGN accretion fueled by a tidally induced gas inflow. For reference, Table 3 lists detected X-ray sources whose position coincides with the optical centre of individual group members, with luminosities of any point-like component derived as described in Section 3. Note that in some cases, such as HCG 97e and most of the *XMM* sources, we cannot clearly distinguish between nuclear and galaxy-wide diffuse

Figure 4. Smoothed 0.3–2 keV images of individual group galaxies showing diffuse X-ray emission. A horizontal bar marks a scale of 1 arcmin in each case.

Table 3. Overview of X-ray sources centred on individual group galaxies as identified by our detection algorithms. Galaxy morphologies were taken from NED. Column 4 lists the unabsorbed 0.3–2 keV luminosity of any nuclear component.

Galaxy	Morph.	Source	$L_{\mathrm{X,nucl}}$ (erg s^{-1})
HCG 7a	Sa	Nuclear?	$3.1 \pm 0.1 \times 10^{40}$
HCG 7b	SB0	Nuclear?	$3.8 \pm 0.4 \times 10^{39}$
HCG 7c	SBc	Nuclear	$4.9 \pm 0.4 \times 10^{39}$
HCG 15a	S0	Nuclear?	$2.6 \pm 0.2 \times 10^{40}$
HCG 15b	S0	Nuclear?	$2.0 \pm 0.2 \times 10^{40}$
HCG 15d	S0	Nuclear?	$6.7 \pm 0.1 \times 10^{41}$
HCG 15e	S0	Nuclear?	$1.9 \pm 0.2 \times 10^{40}$
HCG 30a	SB0	Diffuse	–
HCG 30b	SB0/a	Nuclear	$3.0 \pm 0.4 \times 10^{40}$
HCG 37a	S0/E7	Diffuse + nuclear	$1.4 \pm 0.2 \times 10^{40}$
HCG 37b	Sbc	Nuclear	$0.8 \pm 0.4 \times 10^{39}$
HCG 40a	E	Nuclear	$2.4 \pm 0.5 \times 10^{39}$
HCG 40b	S0	Nuclear	$1.8 \pm 0.4 \times 10^{39}$
HCG 40c	SBb	Diffuse?	–
HCG 40d	SBa	Diffuse? + nuclear	$9.0 \pm 0.9 \times 10^{39}$
HCG 44a	Sa	Diffuse + nuclear	$1.8 \pm 0.2 \times 10^{39}$
HCG 44b	E	Diffuse	–
HCG 44c	SBa	Diffuse	–
HCG 97a	SB0	Diffuse + nuclear	$7.0 \pm 0.8 \times 10^{39}$
HCG 97b	Sc	Nuclear	$1.8 \pm 0.4 \times 10^{39}$
HCG 97c	Sa	Nuclear	$0.9 \pm 0.3 \times 10^{39}$
HCG 97d	E	Diffuse? + nuclear	$8.9 \pm 0.9 \times 10^{39}$
HCG 97e	S0a	Diffuse or nuclear	$0.9 \pm 0.3 \times 10^{39}$
HCG 100a	S0/a	Diffuse + nuclear	$2.7 \pm 0.5 \times 10^{39}$
HCG 100b	S0/a	Diffuse + nuclear	$1.0 \pm 0.3 \times 10^{39}$
Mrk 935	S?	Diffuse or nuclear	$1.6 \pm 0.4 \times 10^{39}$

emission, and the classification of these is followed by a '?' in the Table 3. For HCG 7, however, the tentative identification of nuclear X-ray activity in three of the four principal galaxies agrees perfectly with the *Spitzer* far-infrared results of Gallagher et al. (2008), suggesting our identification is reasonably robust.

Among the principal members in Hickson's (1982) catalogue, we detect 22 candidate nuclear X-ray sources in 40 galaxies, with roughly two-thirds of these falling in the groups with a detectable IGM. The corresponding nuclear source fractions of 64 ± 17 and 44 ± 16 per cent in the groups with and without detectable hot gas, respectively, are statistically indistinguishable at the 1σ level. If instead splitting the sample according to H I deficiency, the corresponding fractions are 42 ± 15 (high Δ_{HI}) and 67 ± 18 per cent, a difference which is only just significant at 1σ. The median nuclear X-ray luminosities for the two subsamples are also very sim-

ilar, 4.4×10^{39} (high Δ_{HI}) and 4.9×10^{39} erg s^{-1}, suggesting that the above conclusions are not strongly biased by a systematic difference in limiting X-ray flux between high– and low-Δ_{HI} groups. We also note that results from optical spectroscopy indicate that ~ 40 per cent of the principal members in HCGs in general show evidence for AGN activity, with a total of ~ 70 per cent showing emission lines from either AGN or star formation activity (Martinez et al. 2007). Our derived fractions are generally bracketed by these values, suggesting that our results give a reasonably reliable picture of the frequency of nuclear activity within our sample.

With the limited statistics available, there is thus no strong evidence from the X-ray data alone for enhanced nuclear activity within a certain kind of groups in our sample. Specifically, if interpreting the X-ray bright or highly H I deficient systems as dynamically more evolved, we find no clear indication that the frequency or strength of nuclear X-ray activity depends on the dynamical status of the group. However, we note that this result applies to a small sample and to the principal members only; a complete census of galaxy membership from optical spectroscopy would be required to extend this analysis to optically fainter group members and place this conclusion on a more robust basis. The tentative lack of a clear enhancement in nuclear X-ray activity among the most H I deficient groups within our sample may tie in with the observation that star formation activity is not globally enhanced in HCG galaxies compared to isolated ones (Verdes-Montenegro et al. 1998), as discussed in more detail in Section 6.

4.3   HI deficiency and IGM properties

The observed diversity in the diffuse X-ray properties of these highly HI deficient groups immediately suggests that galaxy–IGM interactions are not the dominant mechanism for driving cold gas out of the galaxies within our sample and establishing the observed HI deficiencies. Of course, this conclusion neglects the fact that we are not uniformly sensitive to the presence of hot gas in the different groups. A quantitative comparison of observed HI deficiencies and derived IGM properties is therefore presented in Figure 5. The left panel shows $\Delta_{\rm HI}$ and hot IGM mass as listed in Table 2, with both quantities derived within the same region (inside $r_{\rm HI}$ in the Table). Even when considering the X-ray detected systems alone, the obvious lack of a positive correlation between the two quantities immediately suggests that the amount of hot gas in the group core is not a pivotal factor for HI removal. We note that an identical conclusion is reached if replacing $\Delta_{\rm HI}$ with 'missing' HI mass in the plot. The strong 3σ upper limit ($M < 2.6 \times 10^9$ M$_\odot$) on the IGM mass in the highly HI deficient HCG 7 (with the largest 'missing' HI mass in the sample of $\sim 1.8 \times 10^{10}$ M$_\odot$) only reinforces this conclusion. Also note, as pointed out in Section 4.1, that more realistic assumptions about the IGM distribution in the X-ray undetected groups could reduce their upper limits to $M_{\rm IGM}$ by perhaps an order of magnitude, but that this has no bearing on the above conclusions.

Hence, neither is it surprising that $\Delta_{\rm HI}$ does not show a clear dependence on the characteristic IGM ram pressure plotted in Fig. 5b and evaluated as the product of $\sigma_{\rm V}^2$ and the volume-weighted mean IGM density $M_{\rm IGM}/V$ within the volume $V = (4/3)\pi r_{\rm HI}^3$ covered by the radio data, with all quantities taken from Table 2. Note that the very compact HCG 40 – in which we cannot completely rule out a residual galactic contribution to the derived IGM mass – stands out among the X-ray detected groups, with a characteristic ram pressure 1–2 orders of magnitude below that seen in the X-ray bright systems. For the X-ray undetected groups, similar comments apply as for Fig. 5a.

Finally, in Fig. 5c we investigate the dependence of $\Delta_{\rm HI}$ on IGM temperature. Thermal evaporation of galactic HI through heat conduction from the IGM is expected to proceed at a rate $\dot{M} \propto T^{5/2}$ if unsuppressed by, for example, magnetic fields. Given this strong temperature dependence, the lack of a positive $\Delta_{\rm HI}$–T correlation suggests that heat conduction is not an important effect within our sample. The location of the exceptionally HI deficient HCG 30 in Fig. 5c would seem to pose a particular challenge for this mechanism.

Overall, Fig. 5 therefore seems to confirm the notion that HI deficiency is not tightly linked to the presence or nature of an IGM in these groups. There are some caveats to this interpretation though. For example, it is worth emphasizing that it is the four groups with the highest velocity dispersion that are X-ray detected. If the remaining groups contain warm ($T \lesssim 10^6$ K) rather than hot gas, and thus fall well below the σ–T relation for X-ray bright systems, our constraints on the hot gas density could seriously underestimate the true IGM density in these systems. Unfortunately, this possibility cannot be directly tested with the present data. However, the fact that our X-ray detected systems scatter fairly tightly around the Osmond & Ponman (2004) relation, as shown in the inset in Fig. 5c, may support our use of this relation for predicting T also for the undetected systems. Furthermore, results for other X-ray detected groups suggest, if anything, that the poorest systems tend to have T on the high side for their velocity dispersion

(Osmond & Ponman 2004) although the situation could, of course, be different for groups that remain X-ray undetected.

Another concern is that $\sigma_{\rm V}$ and hence $P_{\rm ram}$ in Fig. 5b may not be robustly determined, being based on just a handful of bright galaxies in most cases. Large corrections to $\sigma_{\rm V}$ would be needed, however, in order to affect our overall conclusions. A further point is that any intergalactic HI already stripped from individual galaxies could potentially contribute to the IGM mass and ram pressure. However, for the X-ray detected systems, the *total* HI mass inside the GBT beam is of order 5 per cent of the corresponding hot gas mass (Borthakur et al., in prep.), suggesting that any cold gas can be neglected for the present purposes.

Despite the appearance of Fig. 5, it is premature to exclude the possibility that galaxy–IGM interactions could play a role for HI removal in some of our groups. For example, ram pressure stripping is expected to occur when the IGM ram pressure exceeds the gravitational restoring pressure of the galaxy. The efficiency of this process therefore depends not only on the properties of the IGM, but also on those of the individual group galaxies. The process of viscous stripping (Nulsen 1982) shares similar features, and could be operating even when ram pressure itself is insufficient to remove any HI. Finally, ram pressure may also indirectly affect the HI in the disc. For example, many disc galaxy formation models predict that massive spirals are surrounded by hot gaseous haloes from which gas may cool out to provide fuel for ongoing star formation in the disc (e.g., Toft et al. 2002). The removal of this coronal gas by external forces could contribute to HI deficiency, if the limited supply of HI in the disc is consumed by star formation without being replenished from the hot halo (strangulation; see, e.g., Kawata & Mulchaey 2008). We next seek to quantify the importance of these various mechanisms.

5   THE IMPACT OF THE IGM: MODELLING GALAXY–IGM INTERACTIONS

In an attempt to constrain the role of galaxy–IGM interactions for typical disc galaxies in the individual groups, we constructed simple analytical models of galaxies moving through the hot intragroup gas in the gravitational potential of each group. As explained in Section 4.1, the derived HI deficiency for each group should be viewed as an average for the group members, since it is often nontrivial to evaluate observed HI masses for the individual members. For our modelling purposes, we have therefore adopted a single, fiducial galaxy model, with overall properties broadly matched to the fairly well-constrained mean properties of the late-type group members in our sample.

As described in detail below, the group potential and galaxy orbits are less well determined for each group. Consequently, we evolve the adopted galaxy model according to four different assumptions for each group, corresponding to two choices for the gravitational potential, and two for the galaxy orbits within the chosen potential. The variation among the resulting mass losses from the galaxy can serve as a means to gauge the uncertainties associated with these assumptions. We will consider two different stripping processes for the cold gas in the disc, *viz.* classical ram pressure stripping and turbulent viscous stripping. For the gas in any hot halo, we only consider ram pressure stripping for simplicity.
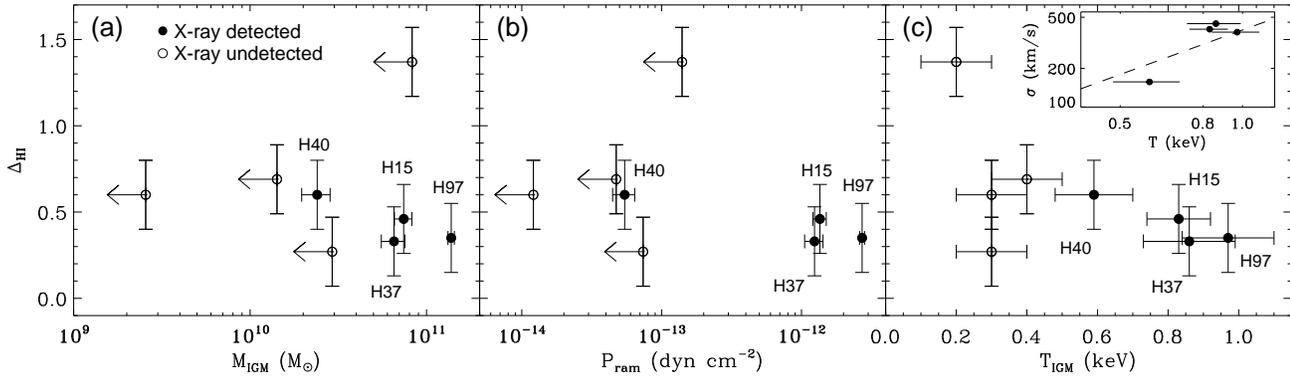
Figure 5. HI deficiency and (a) hot gas mass inside the region used for determining $\Delta_{\rm HI}$, (b) characteristic ram pressure, and (c) hot gas temperature for the various groups. Empty circles represent groups with no detectable hot gas. Inset in (c) shows velocity dispersion vs. $T_{\rm IGM}$ for the X-ray detected groups, with the Osmond & Ponman (2004) relation, i.e. equation (3), overplotted as a dashed line.

5.1 Group model and galaxy orbits

Our goal is to evaluate the efficiency of ram pressure stripping and related processes, without resorting to detailed numerical modelling, which is beyond the scope of this work. For this purpose, we would ideally adopt a single value of the ram pressure for each group. The simplest approach is to assume the classical analytical Gunn & Gott (1972) stripping criterion along with a constant ram pressure equal to its peak value. Hydrodynamical simulations involving a constant ram pressure have shown the Gunn & Gott (1972) criterion to be remarkably accurate in terms of predicting the disc stripping radius and the mass of gas lost (Abadi, Moore & Bower 1999), and it remains a reasonable approximation even when allowing for orbital variations in ram pressure (Jáchym et al. 2007; Roediger & Brüggen 2007).

However, recent hydrodynamical simulations of disc galaxies moving in radial (Jáchym et al. 2007) and two-dimensional orbits (Roediger & Brüggen 2007) within a non-uniform gas distribution have revealed an important exception to this rule. If the ram pressure changes faster than the characteristic stripping time-scale, as will be the case for galaxies moving through a highly concentrated IGM, the Gunn & Gott (1972) criterion tends to overestimates the stripping efficiency. Since stripping is not instantaneous, an ISM element may not always be accelerated to galactic escape velocity before the peak of the ram pressure is over. In such cases the gas will eventually re-accrete, a possibility not taken into account by the Gunn & Gott (1972) criterion. In the present study, these considerations could potentially be relevant for several of our groups, given the fairly small core radii resulting from the surface brightness fits. Instead of using the peak value of the ram pressure in our modelling, it therefore seems more sensible to adopt an orbit-averaged mean ram pressure by evaluating the time spent by the galaxy at a given velocity and IGM density.

To this end, we first derived total mass profiles $M_{\rm tot}(r)$ for each X-ray detected group, assuming a spherically symmetric gas distribution in hydrostatic equilibrium,

$$M_{\rm tot}(<r) = \frac{-kT(r)r}{G\mu m_p} \left(\frac{{\rm d}\ln n(r)}{{\rm d}\ln r} + \frac{{\rm d}\ln T(r)}{{\rm d}\ln r} \right). \tag{4}$$

Since in general we have neither the statistics nor the spatial coverage to constrain $T(r)$ to large radii, we made two assumptions about the temperature profile which are likely to bracket the actual temperature distribution in these somewhat disturbed groups. We either simply assumed $T(r)$ equal to a constant mean value $\langle T \rangle$, or $T(r) = -0.5\langle T \rangle \log(r/r_{500}) + 0.67$, appropriate for reasonably undistorted groups outside any cool core (Rasmussen & Ponman 2007). In the latter case, r_{500}, the radius enclosing a mean density of 500 times the critical value ρ_c, was evaluated iteratively until convergence was reached. For $\langle T \rangle$ we used the measured value listed in Table 2.

The resulting mass profiles were characterized analytically by fitting them with standard 'NFW' models (Navarro, Frenk & White 1997), in which the dark matter distribution is described by

$$\rho(r) = \rho_c \frac{\delta_c}{(r/r_s)(1 + r/r_s)^2}, \tag{5}$$

where δ_c is a dimensionless parameter related to total group mass M_{200}, and r_s is a scale radius which reflects the more commonly used concentration parameter $c = r_{200}/r_s$ (see Navarro et al. 1997 for details). With M_{200}, and hence δ_c, fixed from the measured (extrapolated) mass profile, equation (5) was fitted to this profile to derive values of c under the two assumptions about $T(r)$ described above. The results, summarized in Table 4, imply typical values of $M_{200} \approx 1 - 2 \times 10^{13}$ M$_\odot$ with $c \sim 5 - 10$. For these group masses, derived concentration parameters are thus in good agreement with expectations from cosmological N-body simulations (Bullock et al. 2001). Note that the assumption of a declining temperature profile typically reduces the derived group mass by ~ 30 per cent while increasing the halo concentration by a factor of ~ 2.

For the galaxy orbital configuration within the derived gravitational NFW potential, we assume two different orbits, both radial and hence going through the group core. The galaxy is assumed to be experiencing a face-on IGM encounter in either case. These maximizing assumptions allow us to estimate how important ram pressure stripping can ideally be in our groups. The two orbits differ only in terms of the assumed initial position and velocity of the galaxy, with the galaxy initially at rest at a small clustercentric radius in the first scenario, and falling towards the group core from a large radius and with a high initial velocity in the second. Specifically, the following two scenarios are considered:

(i) For each group, we determine $\bar{r}$, the observed (projected) mean clustercentric distance of the principal galaxies in each group.

Table 4. Results of NFW fits to the derived group mass profiles under the two assumptions for $T(r)$ described in the text.

T isothermal

Group	r_{500} (kpc)	r_{200} (kpc)	M_{200} (10^{13} M$_\odot$)	c
HCG 15	342	541	2.0	4.5
HCG 37	362	572	2.3	4.8
HCG 40	357	565	2.2	4.0
HCG 97	379	500	2.7	4.7

T declining

Group	r_{500} (kpc)	r_{200} (kpc)	M_{200} (10^{13} M$_\odot$)	c
HCG 15	317	474	1.3	10.0
HCG 37	334	499	1.6	11.0
HCG 40	318	474	1.3	9.0
HCG 97	349	523	1.8	10.9

The model galaxy is assumed to be initially at rest at a larger clustercentric distance r_0, from which it falls freely towards the group centre. r_0 is chosen such that when the galaxy reaches $r = \bar{r}$, it has attained a velocity corresponding to the observed group velocity dispersion. Typical values are $r_0 \sim 100$ kpc and $\bar{r} \sim 40$ kpc.

(ii) The galaxy enters the group halo at $r_0 = r_{200}$ with a radial velocity v_r corresponding to the halo circular velocity at this radius, $v_r = (GM/r_{200})^{1/2}$. Typical values are $r_0 \sim 500$ kpc and $v_r \sim 400$ km s^{-1}.

In both cases we follow the galaxy until it turns around, having completed one passage through the group core. The first scenario is chosen in an effort to match the observed average position (modulo projection effects) and galaxy velocity in each group at present. In practice, it represents galaxy motion fairly close to the group core, with a mildly varying ram pressure, and so is somewhat reminiscent of the 'classical' ram pressure scenario involving a constant, high ram pressure. The assumption underlying this orbit is extreme, however, in the sense that the true clustercentric distances will generally be larger than the observed (projected) ones, which implies that galaxies will generally spend a larger fraction of their time at large distance than implied by this assumption. Therefore we also consider scenario (ii) as a kind of opposite extreme. In this, galaxies experience a considerably higher peak ram pressure, but this occurs only relatively briefly. In the following, these two scenarios will be referred to as orbit (i) and (ii), respectively.

Although these two orbits do not necessarily encompass the extreme orbital solutions for the group members, they do represent two rather different cases, thus offering a handle on the uncertainty in the predicted mass loss related to orbital assumptions. Furthermore, while completely radial orbits may not be very common, we note that HI deficient spirals in clusters tend to have more eccentric orbits than non-deficient ones (Solanes et al. 2001), and that cosmological infall along filaments would proceed in fairly eccentric orbits, thus lending some support to our simplifying assumption. For a detailed discussion of the impact of orbital parameters on the stripping efficiency, we refer to Hester (2006).

5.2 Galaxy model

For the galaxy model, needed to estimate the gravitational restoring force and hot halo thermal pressure of a 'typical' late-type group galaxy within our sample, we follow the general approach described in Rasmussen et al. (2006) which is repeated here for completeness. The model consists of a spherical dark matter (DM) halo with density profile

$$\rho_{\rm h}(r) = \frac{M_{\rm h}}{2\pi^{3/2}} \frac{\eta}{r_{\rm t} r_{\rm h}^2} \frac{\exp(-r^2/r_{\rm t}^2)}{(1 + r^2/r_{\rm h}^2)}, \tag{6}$$

a hot gaseous halo of the same form, a spherical bulge with

$$\rho_{\rm b}(r) = \frac{M_{\rm b}}{2\pi r_{\rm b}^2} \frac{1}{r(1 + r/r_{\rm b})^3}, \tag{7}$$

and exponential stellar and gaseous discs, each of the form

$$\rho_{\rm d}(R, z) = \frac{M_{\rm d}}{4\pi R_{\rm d}^2 z_{\rm d}} \exp(-R/R_{\rm d}) {\rm sech}^2(z/z_{\rm d}). \tag{8}$$

Here $M_{\rm b}$, $M_{\rm h}$, and $M_{\rm d}$ are the total masses of each component, $r_{\rm b}$ and $r_{\rm h}$ are the scalelengths of the bulge and halo, respectively, $r_{\rm t}$ is the DM halo 'truncation' radius, $R_{\rm d}$ is the cylindrical scalelength of the disc components and $z_{\rm d}$ the corresponding thickness, and finally

$$\eta = \{1 - \pi^{1/2} q \exp(q^2)[1 - {\rm erf}(q)]\}^{-1}, \tag{9}$$

where $q = r_{\rm h}/r_{\rm t}$ and erf is the error function. With this model, the restoring gravitational acceleration $\frac{\partial \Phi}{\partial z}(R, z)$ in the direction z perpendicular to the disc can be evaluated analytically for each model component using the equations of Abadi et al. (1999), to whom we refer for more details.

In order to constrain model parameters, stellar masses of the HCG members were evaluated from their B- and K-band magnitudes as listed in NED, following the prescription adopted by Mannucci et al. (2005). For this purpose, only the principal members in our eight groups, as listed by Hickson (1982), with morphological types later than S0 were included, yielding a mean stellar mass of 4.1×10^{10} M$_\odot$. For a subset of these galaxies (8 out of 27), maximum disc rotational velocities, indicative of total galaxy masses, are also available in the Hyperleda database, with a mean value of 135 km s^{-1}. We note that, in terms of mean stellar mass, this subset is representative of the full sample, showing $\langle M_* \rangle = 4.4 \times 10^{10}$ M$_\odot$. We therefore assume a stellar mass of 4×10^{10} M$_\odot$ for the galaxy model, distributed such as to yield a bulge-to-disc mass ratio of 1/4, appropriate for an Sb/c spiral. Using the relation of Haynes & Giovanelli (1984), we further assume an HI mass of 6.7×10^9 M$_\odot$ to ensure that our model galaxy initially has a 'normal' HI mass for its sample-averaged blue luminosity of $L_B = 1.6 \times 10^{10}$ L$_\odot$.

The scalelengths of the stellar and gaseous disc components in the model were chosen to ensure that at least 85 per cent of the stellar and HI mass resides within the average optical disc radius of $r_D \simeq 10$ kpc, as derived from the size of the D_{25} ellipse for each spiral member in our groups. For simplicity, the gas distribution in the hot gaseous halo is assumed to follow that of the underlying dark matter, but with a smaller value of r_t corresponding to twice the 'size' r_D of the stellar disc, and with a total mass corresponding to the HI mass in the disc. The hot halo is assumed to be isothermal at a temperature $T \sim 0.06$ keV, the virial temperature corresponding to the maximum allowed disc rotational velocity in the model, taken to be ~ 150 km s^{-1}. Once the baryonic model components have been specified, the parameters of the DM halo are effectively

Table 5. Adopted parameters of the galaxy model. L is the characteristic scalelength for each component, i.e. r_h and r_t for the haloes, r_b for the bulge, and R_d and z_d for the disc components.

Component	M_{total} $(10^{10}\ M_\odot)$	L (kpc)
DM halo	28	5, 100
Hot gas halo	0.7	5, 20
Stellar bulge	0.8	0.5
Stellar disc	3.2	3, 0.25
Cold gas disc	0.67	3, 0.25

set by this maximum allowed rotation velocity, and by the requirement that the model baryon fraction match the universal value of ~ 15 per cent. Table 5 summarises the adopted model galaxy parameters. Note that the cold gas component in the model refers to the distribution of HI only, as we do not consider any molecular gas here. In summary, this model roughly reproduces the average stellar mass, bulge-to-disc ratio, disc size, and maximum disc rotational velocity seen for the spirals in our groups, with a total baryon fraction consistent with the universal value, and an initial HI mass as expected for a non-stripped isolated galaxy with these properties.

5.3 Computing mass losses

Combining equation (5) with the measured density distribution of intragroup gas, time–averaged values of IGM density $\langle \rho \rangle$ and the square of the orbital velocity $\langle v_{\text{gal}}^2 \rangle$ experienced by the galaxy in its orbit can be evaluated. For the averaging time-scale, we only consider the segment of the orbit for which the ram pressure exerts a significant influence on the ISM, taken to be from the time at which the instantaneous ram pressure, if sustained, would remove at least 1 per cent of the cold gas. This is to avoid the artificial suppression of $\langle \rho \rangle$ and $\langle v^2 \rangle$ that would otherwise result from including the time spent by the galaxy at large radius where ram pressure is completely negligible. Note that the corresponding characteristic ram pressure is independent of group mass and orbital initial conditions, as it depends only on the assumed galaxy model.

Assuming a face-on IGM encounter, the condition for ram-pressure stripping is then evaluated as

$$\Sigma_g \left(\frac{\partial \Phi_b}{\partial z} + \frac{\partial \Phi_h}{\partial z} + \frac{\partial \Phi_g}{\partial z} + \frac{\partial \Phi_*}{\partial z} \right) < \langle \rho \rangle \langle v_{\text{gal}}^2 \rangle, \tag{10}$$

where $\frac{\partial \Phi}{\partial z}(R, z)$ is the restoring gravitational acceleration in the direction z perpendicular to the disc, originating from the stellar bulge (subscript 'b'), dark matter halo ('h'), gaseous disc ('g') and stellar disc ('*'), respectively, and Σ_g is the surface density of cold gas. Equation (10) is similar to the classical Gunn & Gott (1972) stripping criterion, but takes into account the mass distribution in the galaxy rather than simply assuming a homogeneous disc thin enough to be described solely by its surface density. Its solution also provides us with the 'stripping region', the region in the (R, z)–plane from which gas is permanently lost by the galaxy.

Apart from conventional ram pressure stripping, transport processes such as viscous stripping (Nulsen 1982), caused by Kelvin–Helmholtz instabilities arising at the ISM–IGM interface, could also play a role even when the ram pressure itself is insufficient to remove galactic gas (Quilis, Moore & Bower 2000; Rasmussen et al. 2006). Turbulent viscous stripping of a gas disc

of radius r_D is expected to operate at Reynolds numbers $Re \gtrsim 30$, where

$$Re = \mathcal{M} r_D / \lambda, \tag{11}$$

$\mathcal{M}$ is the Mach number of the IGM flow past the galaxy, and $\lambda \propto T^2 n^{-1}$ is the ion mean free path in the IGM. The expected mass-loss rate due to this process (Nulsen 1982),

$$\dot{M}_{\text{vs}} \approx 0.5 \pi r_D^2 \rho v_{\text{gal}}, \tag{12}$$

scales only linearly with galaxy velocity and so could be important in a wider range of environments than ram pressure itself. We include this process in the stripping calculations by evaluating equations (11) and (12) at each point in the orbit and adding up the total mass loss. Dealing with disc galaxies rather than spheroids, we have used only half the Nulsen (1982) mass loss rate in equation (12) because of the correspondingly smaller galaxy surface area for a given $r = r_D$. For r_D itself, we use the smaller of the sample-averaged value of $r_D = 10$ kpc and the stripping radius predicted by equation (10). Note that $\mathcal{M} \leqslant 1$ in equation (11) even if the galaxy is moving supersonically, as the post-shock IGM flow past the galaxy will always be subsonic. Also note that the stripping efficiency of both ram pressure and viscous stripping should be largely unaffected by the presence of a shock front (see Rasmussen et al. 2006).

Having dealt with the stripping of cold gas from the disc, we now turn to the removal of any gas situated in a hot galactic halo. It seems plausible that, at the very least, the cooling and gradual inflow of any such gas will be disrupted once the external ram pressure P_{ram} exceeds its thermal pressure P_{th}. The simulations of Mori & Burkert (2000) confirm that this condition provides a reasonable estimate of the mass of a galaxy that will have its hot halo completely stripped by ram pressure. For the purpose of also assessing the importance of strangulation for the model galaxy, we therefore use the derived values of $\langle \rho \rangle$ and $\langle v^2 \rangle$ to evaluate the 'strangulation region' where $P_{\text{ram}} > P_{\text{th}}$, and the corresponding mass of affected coronal gas. The aim here is only to develop a rough picture of the potential importance of IGM interactions for strangulation, so the effects of viscous stripping are not considered for the hot halo.

We readily acknowledge that our modelling approach is inferior to detailed numerical models (e.g., Hester 2006), and hydrodynamical simulations in particular. It is our hope that one can nevertheless have some confidence in the results, given that we have employed a reasonably detailed galaxy model and are making some allowance for orbital variations in ram pressure. The advantage of the adopted method is that it is easily tailored to the specific conditions in individual groups at little computational cost.

5.4 Results

We re-iterate that we are considering four scenarios for each group, consisting of two separate assumptions about the galaxy orbit, and two about the IGM temperature (and hence total mass) distribution in the groups, as specified in Section 5.1. The results of the HI stripping calculations for each of these four cases are summarized in Table 6, which lists the derived r.m.s. orbital velocity v_{rms}, the orbit-averaged IGM number density, the mass of HI lost due to ram pressure and viscous stripping, and the total fraction of HI stripped from the initial model reservoir of $6.7 \times 10^9\ M_\odot$. Recall that v_{rms} is computed only from the point in the orbit where ram pressure becomes significant and so depends not only on orbital parameters but also on the IGM distribution.

Table 6. Orbit–averaged galaxy velocities and IGM densities, along with predicted HI mass loss ΔM due to ram pressure ('rp') and viscous stripping ('vs') after one passage through the group core for the assumed orbits and group mass profiles. The final column lists the total fraction f of HI lost.

Orbit (i), T isothermal

Group	$v_{\rm rms}$ (km s^{-1})	$\langle n \rangle$ (cm^{-3})	$\Delta M_{\rm rp}$ (10^9 M$_\odot$)	$\Delta M_{\rm vs}$ (10^9 M$_\odot$)	f
HCG 15	354	6.7×10^{-4}	0.9	1.0	0.29
HCG 37	342	1.5×10^{-3}	1.2	1.4	0.39
HCG 40	199	7.8×10^{-4}	0.6	0.2	0.12
HCG 97	362	2.6×10^{-3}	1.6	2.3	0.58

Orbit (i), T declining

Group	$v_{\rm rms}$ (km s^{-1})	$\langle n \rangle$ (cm^{-3})	$\Delta M_{\rm rp}$ (10^9 M$_\odot$)	$\Delta M_{\rm vs}$ (10^9 M$_\odot$)	f
HCG 15	404	7.2×10^{-4}	1.0	0.9	0.29
HCG 37	402	1.9×10^{-3}	1.4	1.2	0.39
HCG 40	266	8.2×10^{-4}	0.8	0.2	0.14
HCG 97	435	2.8×10^{-3}	1.8	2.0	0.57

Orbit (ii), T isothermal

Group	$v_{\rm rms}$ (km s^{-1})	$\langle n \rangle$ (cm^{-3})	$\Delta M_{\rm rp}$ (10^9 M$_\odot$)	$\Delta M_{\rm vs}$ (10^9 M$_\odot$)	f
HCG 15	498	1.2×10^{-4}	0.6	1.2	0.27
HCG 37	541	1.5×10^{-4}	0.7	1.9	0.39
HCG 40	630	4.3×10^{-5}	0.5	0.3	0.12
HCG 97	536	2.8×10^{-4}	0.9	4.3	0.77

Orbit (ii), T declining

Group	$v_{\rm rms}$ (km s^{-1})	$\langle n \rangle$ (cm^{-3})	$\Delta M_{\rm rp}$ (10^9 M$_\odot$)	$\Delta M_{\rm vs}$ (10^9 M$_\odot$)	f
HCG 15	448	1.2×10^{-4}	0.5	1.2	0.26
HCG 37	491	1.5×10^{-4}	0.6	1.9	0.38
HCG 40	554	4.6×10^{-5}	0.4	0.3	0.11
HCG 97	477	2.8×10^{-4}	0.8	4.3	0.76

As can be seen from the Table, the amount of gas lost through either stripping process is generally an appreciable fraction of the initial HI mass. Viscous stripping in particular can remove a substantial fraction of the cold disc gas for all model assumptions. HCG 40 is the exception, with the relatively tenuous IGM in this group removing at most 10–15 per cent of the HI. The steeper IGM density profile in this group also implies that a larger fraction of the total IGM mass is encountered at high velocity, leading to a higher $\Delta M_{\rm rp}/\Delta M_{\rm vs}$ ratio than for the other groups, and a higher value of $v_{\rm rms}$ in orbit (ii), because the ram pressure becomes significant closer to the core in this system.

The Table further shows that the main variation in the computed mass loss for a given group and stripping mechanism derives from the choice of orbit rather than the assumed group mass profile. Orbit (i) is generally more efficient at removing gas through ram pressure stripping than orbit (ii), because although the peak ram pressure is considerably higher in the latter case, the galaxy spends a comparatively shorter time in regions corresponding to high values of $P_{\rm ram}$. Conversely, viscous stripping is more efficient in orbit (ii), as this mechanism acts even at relatively low $v_{\rm gal}$, allowing the associated mass loss to build up significantly over the much longer crossing time-scale relevant for this orbit. Note, how-
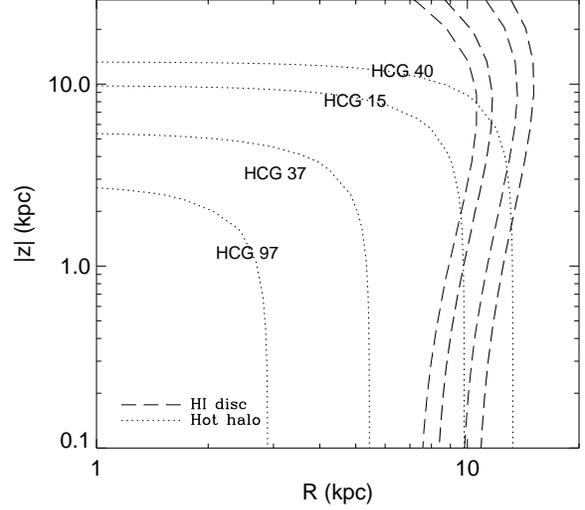

Figure 6. Isobars of gravitational restoring pressure (dashed) and hot halo thermal pressure (dotted) for our fiducial model galaxy in the different groups. Dashed lines outline the galactic regions outside which HI in the disc can be stripped by ram pressure, corresponding to equality in equation (10). Dotted lines show the corresponding regions for the hot halo gas. The order of the contours is the same in both cases.

ever, that for a given group, the outcome in terms of *total* HI mass loss, $\Delta M_{\rm tot} = \Delta M_{\rm rp} + \Delta M_{\rm vs}$, is largely insensitive to the various orbit and mass profile assumptions, despite clear variations in $\langle n \rangle$ and $v_{\rm rms}$ among the four scenarios. The only exception to this is the significantly more massive HCG 97, for which the deeper gravitational potential and higher IGM mass implies that orbit (ii) is relatively more efficient at removing galactic gas than for the other groups.

Figure 6 outlines the stripping region for a model galaxy in each of the X-ray detected groups, based on solving equation (10). The figure shows the one of our four scenarios in which the effect of ram pressure is generally most pronounced, i.e., orbit (i) with $T(r)$ declining. In the outer disc, the gravitational restoring pressure, and hence the stripping region for the cold gas, is seen to be nearly independent of vertical disc height for interesting values of $|z|$, and the gravitational restoring force at a given R peaks well above the disc. Compared to the 'size' of the stellar disc ($r_D = 10$ kpc), it is clear that the gas disc becomes mildly truncated by ram pressure in HCG 97 and 37 but remains largely unaffected in the other two groups. Note that this truncation reduces the viscous stripping efficiency by reducing the surface area of the gas disc exposed to the IGM. Viscous stripping is therefore slightly more efficient for low values of $P_{\rm ram}$, adding to the explanation of the higher values of $\Delta M_{\rm vs}$ for orbit (ii) in Table 6.

Predicted HI deficiencies corresponding to the mass losses in Table 6 are compared to the observed values in Fig. 7. Errors on predicted deficiencies correspond to the full range in predicted HI mass loss for each group under the various orbit and mass profile assumptions. Shown are the expectations from ram pressure stripping alone, as well as the full HI mass loss from combining equations (10) and (12). The dashed line in the figure represents equality between modelled and observed HI deficiencies; under our model assumptions, anything below this line cannot be explained by galaxy–IGM interactions alone. The plot clearly suggests that ram pressure stripping on its own is not sufficient to cause the ob-
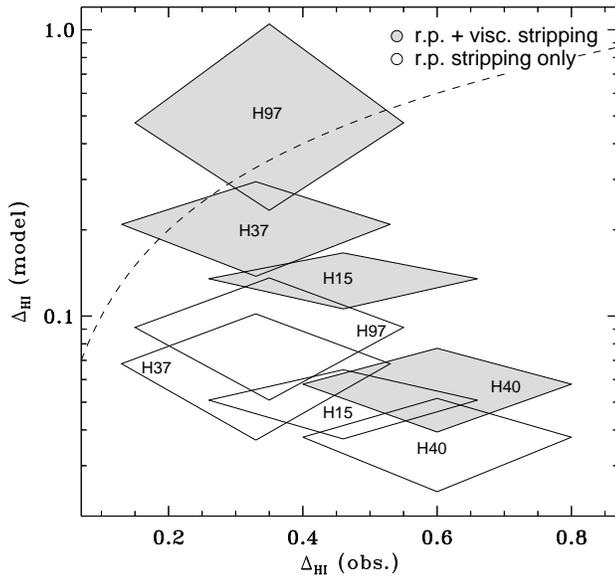
Figure 7. Observed H I deficiencies compared to the model predictions of Table 6 for the stripping of H I by ram pressure alone (empty diamonds), and by ram pressure plus viscous stripping (shaded). Dashed line represents equality between observed and predicted Δ_{HI}.

Table 7. Fraction of hot halo gas lost due to ram pressure in the various orbital scenarios.

Group	Orbit (i) $T(r)$ const.	Orbit (i) $T(r)$ decl.	Orbit (ii) $T(r)$ const	Orbit (ii) $T(r)$ decl.
HCG 15	0.53	0.64	0.31	0.27
HCG 37	0.74	0.85	0.39	0.35
HCG 40	0.31	0.46	0.21	0.18
HCG 97	0.84	0.94	0.52	0.48

served H I deficiencies, even in this X-ray bright subsample of our groups. When including viscous stripping, however, if as efficient in removing H I as assumed here, galaxy–IGM interactions can certainly help explain observed values of Δ_{HI}, but they can potentially fully account for the H I loss only in HCG 37 and HCG 97, i.e. in just two out of our eight groups.

Regarding the issue of strangulation, Fig. 6 also illustrates the derived stripping region for hot halo gas according to the adopted $P_{ram} > P_{th}$ criterion. The figure suggests that ram pressure alone could remove a sizable fraction of the halo gas in the model. Table 7 lists the fractions of stripped halo gas in the different scenarios, showing that these can be substantial for orbit (i) in particular, peaking at ~ 95 per cent in HCG 97. Viscous stripping, not included here, could potentially contribute beyond these estimates. This suggests that galaxy–IGM interactions in X-ray bright groups could play an important role in removing the gas supply that may ultimately fuel star formation in spirals, in qualitative agreement with the simulation results of Kawata & Mulchaey (2008). For our specific model setup, there is a large dispersion in the fraction of gas affected, however, and it is not clear that the effect would be important in groups such as HCG 40.

5.5 Model limitations and caveats

It is important to stress that the calculations presented here are only intended to provide a rough picture of the impact of galaxy–IGM interactions in our sample, and we do not claim that these results are anything but indicative. Caveats include the fact that the adopted galaxy model parameters provide a plausible, but not necessarily unique, representation of the spirals in our sample. It is also a possibility, albeit one we cannot easily evaluate, that some group members may be individually less H I deficient than the 'group-averaged' value of Δ_{HI}, and so could have H I deficiencies consistent with removal by ICM interactions alone, even if our model results suggest otherwise for the group members as a whole.

As regards the model calculations, an important limitation is the fact that the model is completely static. In practice, the gas distributions both in the groups and their galaxies will be evolving, which could be particularly relevant for orbit (ii) where orbital time-scales are several Gyr. Also, the estimate of viscous stripping mass loss does not take into account that this process itself will reduce the size of the gas disc and hence the mass loss rate according to equation (12). Furthermore, this stripping process may saturate (Nulsen 1982) which would reduce the mass loss, the presence of magnetic fields could also suppress hydrodynamical instabilities, and the presence of a hot halo could perhaps to some extent shield the cold gas disc from such instabilities. The latter could be of particular relevance for orbit (ii), in which ΔM_{vs} is high but where a comparatively smaller fraction of halo gas is lost due to ram pressure. These considerations suggest that the estimated contribution by viscous stripping to the H I mass loss should be regarded as an upper limit.

With their compact galaxy configurations and low velocity dispersions, our groups could also represent environments in which galactic dark matter haloes are subject to significant tidal truncation. Hence, another issue is to what extent our results are affected by the adopted assumptions on dark matter in the galaxy model. For the adopted disc and bulge parameters, our freedom to modify the assumed DM distribution is mainly constrained by the requirement that the maximum disc rotational velocity v_{max} of the model should not exceed the allowed ~ 150 km^{-1}. A full exploration of model parameter space is beyond the scope of this work, and we refer to Hester (2006) for a more thorough investigation of these issues. Nevertheless, to provide a rough picture of the impact of DM for our results, we repeated the stripping calculations of Section 5.3 with three different modifications, subject to the above v_{max} criterion:

(i) Assuming no DM [or larger DM halo scalelengths r_t and r_h in equation (6)]. This must be regarded as an extreme assumption, which should facilitate stripping.
(ii) Increasing the DM mass by a factor of two (for which the v_{max} criterion then requires at least one of the DM scalelengths r_t and r_h to increase by a similar factor). This should suppress stripping.
(iii) Assuming a higher DM concentration (i.e. lower r_h or r_t) by a factor of three (suppresses stripping), which in turn requires a lower total DM mass by a factor of five (facilitates stripping). These choices comply with the typical tidal truncation of DM halos inferred for galaxies in massive clusters (Limousin et al. 2007).

We find that, in all three cases, the amount of H I lost by the model galaxy is at most modified by 10–15 per cent, regardless of the group and orbit considered. This perhaps somewhat surprising result has its origin in the fact that the vast majority of cold gas in the model is located at low galactocentric distances, where the

restoring gravitational acceleration – which determines the stripping region in accordance with equation (10) – is dominated by the baryonic disc components and not the dark matter halo. The variations in the stripped gas mass for the hot halo can be larger, up to 45 per cent for HCG 40, but they can generally easily be accommodated by the variations associated with the different orbital assumptions. We therefore conclude that our results are reasonably robust to changes in the assumed amount and distribution of dark matter in the galaxy model.

6   DISCUSSION

The groups in our sample are all H I deficient even when accounting for any intergalactic H I not clearly associated with individual galaxies. Removal of H I from the group members is by itself insufficient to explain this situation, as the removed gas must also be prevented from staying neutral. Thus, unless H I is somehow destroyed *in situ* within the galaxies, it must go through a two-stage process whereby it is first removed from the galaxies and then ionized by a possibly unrelated mechanism. Here we discuss these different possibilities in light of our X-ray and modelling results.

6.1   *In situ* destruction of H I

The H I could potentially have been destroyed within the galaxies themselves, either by evaporation though thermal conduction from the IGM, or through consumption by star formation, provided there is no continuous replenishment of cold material. A third possible mechanism involves heating and possibly ejection from the galaxies by starburst winds. While the first possibility, direct heating by the IGM, seems implausible in light of the absence of a positive correlation between Δ_{HI} and T_{IGM} (cf. our discussion of Fig. 5c), the two other scenarios deserve some further attention. H I consumption by star formation could help establish observed deficiencies, but a prerequisite is that the consumed gas is not simply replenished at a similar rate, for example through the cooling out of hot, coronal material on to the disc. Our model results for the X-ray bright groups (Table 7) suggest that such a strangulation scenario could at least be greatly facilitated by the removal of coronal gas due to ram pressure, but a more detailed exploration of model parameter space would be required to assess the general validity of this conclusion.

In this context, it is instructive to compare the results from our simple analytical model to the simulation results of Kawata & Mulchaey (2008). These authors investigate the efficiency of ram pressure stripping and strangulation for a galaxy in a small galaxy group on the basis of a cosmological smoothed particle hydrodynamics (SPH) simulation. They do not specifically consider a 'compact' group, but this has the advantage that their target galaxy is not subject to noticeable gas loss from tidal interactions (D. Kawata, priv. comm.), so in this sense a comparison to our model calculations is justified. Their target galaxy has initial properties broadly similar to those of our galaxy model in terms of stellar, gaseous, and total mass. It is followed for one passage through the group as it enters a group of virial mass $M \approx 8 \times 10^{12}$ M$_\odot$ from an initial position roughly corresponding to twice the virial radius. The galaxy orbit thus shows some similarities to our orbit (ii), but, with a pericentre at $r \sim 200$ kpc, does not take the galaxy through the very core of the IGM distribution. Kawata & Mulchaey (2008) find that the resulting ram pressure induces strangulation to a significant degree. Star formation and thus H I consumption becomes mildly enhanced during infall, and the hot halo gas is almost

completely removed during the group passage. The combination of these processes has effectively consumed the H I and quenched star formation by the time the galaxy re-emerges at the virial radius.

Our model conclusion that ram pressure stripping may strongly affect any coronal gas in the X-ray bright groups is thus in encouraging agreement with these simulation results, and it is even possible that our model underestimates the importance of ram pressure in this context. This is made more relevant still if ram pressure – or other galaxy interactions with the group environment – indirectly accelerate strangulation by enhancing the disc star formation rate and hence the consumption of H I. This possibility draws observational support from the strong star formation activity seen in the ram-pressure affected group spiral NGC 2276 (Rasmussen et al. 2006), as well as from recent hydro-simulations (Kronberger et al. 2008). However, Verdes-Montenegro et al. (1998) noted on the basis of star formation rates derived from *IRAS* far-infrared luminosities that there is no indication of enhanced star formation among the HCG galaxies compared to the level seen in isolated galaxies. In fact, current star formation rates in these groups generally seem too low to explain the missing H I by consumption through star formation. For the spirals in our sample, a mean star formation rate of $\dot{M}_* \approx 1.4$ M$_\odot$ yr^{-1} can be derived for the *IRAS*-detected galaxies. However, many of our galaxies remain undetected in one or more *IRAS* bands and so have only upper limits to $\dot{M}_*$ (if including these upper limits in the mean, the result is $\dot{M}_* < 0.9$ M$_\odot$ yr^{-1}). At these rates, the time-scale for star formation to exhaust an initial H I supply of 6.7×10^9 M$_\odot$ to current levels is at least 5 Gyr, even if neglecting the return of unprocessed material to the ISM *and* any cosmological accretion of gas by the galaxy.

Thus, while our model calculations and the results of Kawata & Mulchaey (2008) suggest that hot halo gas can be removed fairly efficiently in several of our groups, potentially inhibiting or at least suppressing any replenishment of disc H I from a hot halo, strangulation does not seem to have played an important role in establishing current H I levels within our sample. At the observed star formation rates, the remaining H I can continue to fuel star formation for many Gyr without drastically reducing the H I supply. Of course, star formation rates could have been much higher in the past, which could also indirectly have contributed to exhausting the gas supply through the ejection of gas from the disc by starburst winds. However, unless $\dot{M}_*$ in these galaxies has generally declined to current levels only fairly recently or has been affected by the group environment over cosmological time-scales, the implication seems to be that destruction of neutral hydrogen within the galaxies themselves cannot explain the H I deficiencies. The presence of intergalactic H I in some of our groups also shows that this scenario cannot provide an exhaustive explanation. We are therefore compelled to also consider the alternative, externally–driven removal and destruction of H I.

6.2   H I removal by external forces

Focussing first on the removal of H I, both galaxy–IGM and galaxy–galaxy interactions could be envisaged to play a role. Our results demonstrate that although earlier studies indicated a link between significant H I deficiency in Hickson groups and the presence of hot intragroup gas (Verdes-Montenegro et al. 2001), there is clearly no one-to-one correspondence between the two. The lack of a detectable intragroup medium inferred here for half of the eight most H I deficient compact groups specifically appears to rule out IGM dynamical interactions as generally dominant for H I removal within these environments. Ram pressure and viscous stripping

could nevertheless still have played a role for H I removal in our X-ray detected systems. Our modelling results indicate, however, that the efficiency of these processes is generally insufficient to fully account for the H I missing from the individual group members, especially if our simplistic treatment of viscous stripping overestimates the predicted H I loss, as hypothesized in Section 5.5.

Overall, the simulations of Kawata & Mulchaey (2008) seem to support these conclusions. In these, ram pressure affects the amount of cold gas in the disc to an even lesser degree than in our model, although this could perhaps be attributed to the fact that our groups are at least twice as massive, and perhaps also to the maximizing orbital assumptions adopted in our model. Viscous stripping does not appear to be important in the simulations, but as noted by Kawata & Mulchaey (2008), such processes are not necessarily well treated by SPH schemes, so a direct comparison to our results may not be meaningful.

The limited impact of galaxy–IGM interactions inferred for our groups commands an alternative explanation for the H I removal. Tidal stripping constitutes an obvious candidate in these dense, low-σ environments, particularly in light of the fact that the four X-ray undetected groups within our sample exhibit the lowest velocity dispersions and so could be expected to represent environments where tidal interactions should be most important. However, even if for now ignoring the problem of subsequently heating the removed H I, it is not immediately clear that tidal interactions would necessarily result in increased H I *deficiency*, as they would also affect the stellar component in the galaxies. If stars and gas are removed in roughly equal proportion, and if the removed stars become part of any undetected intracluster light (cf. Gonzalez, Zaritsky & Zabludoff 2007) while the H I remains detectable, this could potentially even result in an H I excess. Recalling that H I deficiency is defined here on the basis of the observed B-band galaxy luminosity, increasing Δ_{HI} through tidal stripping therefore requires either the preferential removal of cold gas compared to stars (and its subsequent heating), or that L_B is simultaneously boosted relative to the H I mass for the non-stripped components.

The latter possibility gains support from the observation that specific star formation rates generally tend to be higher in galaxies with close neighbours (Li et al. 2008), with enhanced nuclear star formation plausibly arising as a consequence of tidally induced gas inflow. It is perhaps curious then, as mentioned above, that there is no evidence for enhanced star formation in Hickson groups compared to the level in isolated galaxies. This runs contrary to expectations for interacting galaxies, and would seem to argue against L_B being significantly boosted in the HCG members relative to their remaining stellar or H I mass. The other possibility mentioned above, that H I is more easily tidally stripped than the stellar component, is perhaps more promising. In many of our groups, such as HCG 100 (cf. Section 4.1.8), significant amounts of intergalactic H I is detected with the GBT, whereas the stellar components are not noticeably affected. A possible explanation is that a relatively larger fraction of H I compared to stars initially resided at large galactocentric radii, where tidal removal would be most efficient. The fact that the H I disc in typical spirals and late-type dwarfs is often more extended than its optical counterpart, with the radial distribution of H I declining less steeply with radius than that of the B-band light (Broeils & Rhee 1997; Swaters et al. 2002), seems to support such an explanation.

Tidal stripping clearly *is* taking place in some of our groups, notably in the X-ray undetected groups HCG 100 and HCG 44. In the latter, both optical (Fig. 1) and H I data (Borthakur et al., in prep.) show strong evidence for the SBc galaxy HCG 44d being tidally stripped. This may indicate that tidal stripping is the primary mechanism by which H I is removed from the galaxies in these two groups. Although it is tempting to extend this conclusion to all the X-ray undetected groups in our sample, and perhaps even beyond, the inconspicuous star formation rates in Hickson groups in general, and the tentative lack of enhanced nuclear X-ray activity in the highly H I deficient systems in particular (Section 4.2), may not argue in favour of such an explanation.

6.3 Destruction of removed H I

As emphasized in the beginning of this Section, H I deficiencies can only be explained if the hydrogen, once removed from the group members, is also transformed from its neutral phase. Irrespective of the processes accomplishing its removal, a mechanism must therefore also be invoked for ionizing the H I during or following its transfer to intergalactic space. In our X-ray bright groups, a candidate process is readily available, since any removed H I is expected to evaporate due to heating by the ambient IGM at a rate $\dot{M} \propto T^{5/2}$, almost independently of realistic values of the IGM density (Spitzer 1962). A detailed comparison of the X-ray and H I properties of these groups should help test this explanation and will be presented elsewhere (Verdes-Montenegro et al., in prep.). In the X-ray undetected groups, where any IGM is expected to be relatively cool (cf. Fig. 5c) if at all present, the picture is less clear-cut. Even if these groups do contain an IGM, the lower predicted IGM temperatures in this subsample imply average IGM heating time-scales an order of magnitude above those in the X-ray bright systems, casting doubt on whether this mechanism would be sufficient.

If gas is predominantly removed by tidal interactions in the X-ray undetected groups, it is instead conceivable that some of the H I has been heated by tidal shocks, although the presence of intergalactic H I in some of the groups would imply heating time-scales well in excess of those associated with the H I removal itself. Another possibility is that the column density of any removed H I becomes too low for the gas to be self-shielding against ionization by cosmic UV radiation. If so, much of the undetected hydrogen in these groups could potentially be in the form of a tenuous, photoionized intergalactic plasma. A quantitative investigation of these possibilities is the subject of future work, but at present a clear picture of the fate of the removed H I in the X-ray undetected groups remains elusive.

7 CONCLUSIONS

Based on a sample of eight Hickson compact groups selected for their high H I deficiencies, we have used *Chandra* and *XMM-Newton* data to assess the properties of any hot intragroup medium (IGM) and constrain the role of galaxy–IGM interactions in removing H I from the galaxies in these groups. The X-ray analysis reveals a detectable IGM in four of the eight groups. We have tentatively identified the detected diffuse emission in HCG 40, a spiral-dominated group, as associated with an intragroup medium, but the combination of a low signal-to-noise ratio and an exceptionally compact galaxy configuration precludes a highly robust conclusion for this particular system. The remaining three groups are all fairly X-ray luminous, showing substantial amounts of intergalactic hot gas with a somewhat disturbed morphology in all cases.

The remarkable X-ray diversity seen across the sample immediately suggests that the presence of a significant IGM is not a dominant factor in establishing observed HI deficiencies, despite earlier results indicating such a connection (Verdes-Montenegro et al. 2001). It is particularly notable that some of the most HI deficient groups show no detectable hot IGM, including HCG 30 which only contains a few per cent of the expected HI mass for its galaxy content. A comparison of HI deficiency with either hot IGM mass or characteristic 'mean' ram pressure confirms the lack of a clear correlation even for the X-ray bright systems, although statistics are naturally too limited to enable firm conclusions on this basis alone. The HI deficiency does not seem to depend on IGM temperature either, suggesting that heat conduction from the IGM does not play an important role in destroying galactic HI (although once removed, this gas is likely to evaporate on fairly short time-scales in the X-ray bright groups).

From fitting analytical models to the derived mass profiles of the X-ray detected groups, we have constructed plausible models of the gravitational potential and associated radial galaxy orbits for each of these groups. Combined with the inferred IGM distributions and a numerical model of a late-type galaxy with properties broadly matching those of our observed spirals, this has enabled estimates of the importance of ram pressure stripping and viscous stripping in removing HI from the late-type galaxies in each group. The results indicate that, even under maximizing assumptions about the galaxy orbit, ram pressure stripping will remove only small amounts of cold gas from the group members, peaking at 10–25 per cent in the X-ray bright HCG 97. We find that viscous stripping is generally more efficient, with the combination of the two processes capable of removing more than half of the cold ISM in HCG 97 and potentially fully accounting for the missing HI mass in both HCG 37 and HCG 97. However, the efficiency of viscous stripping is likely overestimated with our simple analytical approach, and yet these processes are insufficient in terms of explaining the HI deficiency of the X-ray detected HCG 15 and HCG 40.

The model results also indicate that ram pressure can efficiently remove a large fraction of any hot galactic halo gas that may otherwise act as a supply of fresh material for star formation in the disc. However, even if the gas supply to the disc can be completely cut off, gas consumption at the typical star formation rates in the groups would proceed far too slowly to explain the observed shortfall of HI by itself. Much higher star formation rates in the recent past are required for this process to have had any significant impact. This may suggest that the observed HI deficiencies are not caused by *in situ* destruction of HI within the galaxies themselves. It remains a possibility that even modest star formation activity could have heated some of the HI and lifted it above the disc midplane where it would be more susceptible to removal by ram pressure, similar to the situation proposed for NGC 2276 (Rasmussen et al. 2006). The absence of observational signatures of this process, e.g., in the form of a hot gas tail extending from any of the group members, may suggest that such a mechanism is not generally very important within our sample though.

By the process of elimination, it seems plausible that tidal interactions have played a key role for HI removal in the groups, particularly in those systems containing no detectable IGM. In order to explain the HI *deficiencies*, this scenario would likely require preferential removal of HI over stars, as perhaps facilitated by the more extended distribution of cold gas relative to stars in typical late-type galaxies. While it is perhaps not surprising that tidal interactions are affecting the gas content of galaxies in these compact groups, the tidal stripping explanation still faces some outstanding

issues. Among these is the expectation that such interactions would generate enhanced star formation or nuclear activity, but there is no indication that the X-ray faint or highly HI deficient systems in our sample show evidence for increased such activity (although the frequency of nuclear activity in galaxies in compact groups in general may be rather high; Martinez et al. 2007). If interpreting the X-ray bright or highly HI deficient systems within our sample as dynamically more evolved, we thus find no clear evidence that the frequency or strength of nuclear X-ray activity in the group members depends on the dynamical status of the group. It also remains unclear whether tidal interactions themselves can destroy the HI during or following its removal from galactic discs and so fully explain the HI deficiency in any of our groups.

In closing, our results suggest that galaxy–IGM interactions can have played a role for the removal and destruction of HI in some of our groups, but a complete understanding of the origin of the observed HI deficiencies and the processes causing it is still lacking. Strangulation or thermal evaporation do not emerge as important contenders, and typical indirect signatures of tidal interactions, such as enhanced star formation or nuclear X-ray activity, are not more pronounced within the more HI deficient half of our sample. The latter seems in line with previous results (Verdes-Montenegro et al. 1998) which indicate that star formation rates in Hickson compact groups are not globally enhanced relative to the field. We note here that this result could potentially be misleading, however, perhaps masking an evolutionary trend in which galaxies initially experience enhanced star formation which is then followed by an environment–driven suppression. A detailed correlation of HI and X-ray morphology in the groups, coupled with a broad comparison of individual galaxy properties such as specific star formation rates, may therefore shed further light on the fate of the missing HI in these compact systems. This is the subject of future work.

REFERENCES

Abadi M. G., Moore B., Bower R. G., 1999, MNRAS, 308, 947
Arnaud M., et al., 2002, A&A, 390, 27
Broeils A. H., Rhee M.-H., 1997, A&A, 324, 877
Bullock J. S., Kolatt T. S., Sigad Y., Somerville R. S., Kravtsov A. V., Klypin A. A., Primack J. R., Dekel A., 2001, MNRAS, 321, 559
Cortese L., Gavazzi G., Boselli A., Franzetti P., Kennicutt R.C., O'Neil K., Sakai S., 2006, A&A, 453, 847
Coziol R., Plauchu-Frayn I., 2007, AJ, 133, 2630

Dickey J.M., Lockman F.J., 1990, ARA&A, 28, 215

Dos Santos S., Mamon G. A., 1999, A&A, 352, 1

Fukazawa Y., Kawano N., Ohta A., Mizusawa H. 2002, PASJ, 54, 527

Gallagher S. C., Johnson K. E., Hornschemeier A. E., Charlton J. C., Hibbard J. E., 2008, ApJ, 673, 730

Giovanelli R., Haynes M.P., 1985, ApJ, 292, 404

Gonzalez A. H., Zaritsky D., Zabludoff A. I., 2007, ApJ, 666, 14

Grevesse N., Sauval A.J., 1998, Space Sci. Rev., 85, 161

Gunn J.E., Gott J.R. III, 1972, ApJ, 176, 1

Haynes M.P., Giovanelli R., 1984, AJ, 89, 758

Helsdon S.F., Ponman T.J., 2003, MNRAS, 339, L29

Hester J. A., 2006, ApJ, 647, 910

Hickson P., 1982, ApJ, 255, 382

Jáchym P., Palouš J., Köppen J., Combes F., 2007, A&A, 472, 5

Kawata D., Mulchaey J.S., ApJL, 672, L103

Kronberger T., Kapferer W., Ferrari C., Unterguggenberger S., Schindler S., 2008, A&A, in press (arXiv:0801.3759)

Lewis I., et al., 2002, MNRAS, 334, 673

Li C., Kauffmann G., Heckman T., Jing Y. P., White S. D. M., 2008, MNRAS in press (arXiv:0711.3792)

Machacek M. E., Nulsen P., Stirbat L., Jones C., Forman W. R., 2005, ApJ, 630, 280

Limousin M., Kneib J.P., Bardeau S., Natarajan P., Czoske O., Smail I., Ebeling, H., Smith G.P., 2007, A&A, 461, 881

Mahdavi A., Finoguenov A., Böhringer H., Geller M.J., Henry J.P., 2005, ApJ, 622, 187

Mannucci F., Della Valle M., Panagia N., Cappellaro E., Cresci G., Maiolino R., Petrosian A., Turatto M., 2005, A&A, 433, 807

Martinez M. A., Del Olmo A., Perea J., Coziol R., 2007, in Saviane I., Ivanov V.D., Borissova J., eds, Groups of Galaxies in the Nearby Universe, Springer-Verlag, Berlin, p. 163

Mori M., Burkert A., 2000, ApJ, 538, 559

Mulchaey J.S., Davis D.S., Mushotzky R.F., Burstein D., 2003, ApJS, 145, 39

Navarro J. F., Frenk C. S., White, S. D. M., 1997, ApJ, 490, 493

Nulsen P.E.J., 1982, MNRAS, 198, 1007

Osmond J. P. F., Ponman T. J., 2004, MNRAS, 350, 1511

O'Sullivan E., Ponman T. J., Collins R. S., 2003, MNRAS, 340, 1375

Ponman T.J., Bourner P.D.J., Ebeling H., Böhringer H., 1996, MNRAS, 283, 690 (P96)

Quilis V., Moore B., Bower R., 2000, Science, 288, 1617

Rasmussen J., Ponman T. J., 2007, MNRAS, 380, 1554

Rasmussen J., Ponman T.J., Mulchaey J.S., 2006, MNRAS, 370, 453

Rasmussen J., Stevens I.R., Ponman T.J., 2004, MNRAS, 354, 259

Read A.M., Ponman T.J., 2001, MNRAS, 328, 127

Read A.M., Ponman T.J., 2003, A&A, 409, 395

Roediger E., Brüggen M., 2007, MNRAS, 380, 1399

Sengupta C., Balasubramanyam R., 2006, MNRAS, 369, 360

Solanes J.M., Manrique A., García-Gómez C., González-Casado G., Giovanelli R., Haynes M.P., 2001, ApJ, 548, 97

Spitzer L., 1962, Physics of Fully Ionized Gases, Interscience, New York, NY

Sun M., Vikhlinin A., 2005, ApJ, 621, 718

Sutherland R.S., Dopita M.A., 1993, ApJS, 88, 253

Swaters R. A., van Albada T. S., van der Hulst J. M., Sancisi R., 2002, A&A, 390, 829

Toft S., Rasmussen J., Sommer-Larsen J., Pedersen K., 2002, MN-RAS, 335, 799

Trinchieri G., Sulentic J., Breitschwerdt D., Pietsch W., 2003, A&A, 401, 173

Verdes-Montenegro L., Yun M.S., Perea J., del Olmo A., Ho P.T.P., 1998, ApJ, 497, 89

Verdes-Montenegro L., Yun M.S., Williams B.A., Huchtmeier W.K., Del Olmo A., Perea J., 2001, A&A, 377, 812

Vikhlinin A., Markevitch M., Murray S. S., Jones C., Forman W., Van Speybroeck L., 2005, ApJ, 628, 655

Wang Q. D., Owen F., Ledlow M., 2004, ApJ, 611, 821

Williams B.A., Rood H.J., 1987, ApJS, 63, 265

Yang X., Mo H. J., van den Bosch F. C., Pasquali A., Li C., Barden M., 2007, ApJ, 671, 153

This paper has been typeset from a TEX/ LATEX file prepared by the author.